View metadata, citation and similar papers at core.ac.uk
brought to you by CORE
provided by IUPUIScholarWorks

PHOTO-CURING THROUGH SINGLE APERTURES:

THE PHENOMENON AND ITS INFLUENCE ON POLYMERIZATION

Meoghan Elizabeth MacPherson

Submitted to the faculty of the University Graduate School
in partial fulfillment of the requirements
for the degree
Master of Science
in the School of Dentistry,
Indiana University

June 2013

Accepted by the Faculty of Indiana University, in partial fulfillment of the requirements for the degree of Master of Science.

Master's Thesis Committee

Tien-Min Gabriel Chu, D.D.S., Ph.D., Chair

Jeffrey A. Platt, D.D.S., M.S.

B. Keith Moore, Ph.D.

David T. Brown, D.D.S., M.S.

Christoph A. Naumann, Ph.D.

DEDICATION

This thesis is dedicated to Barbara Rhodes; a woman whose insight, guidance, and encouragement when this journey first began transcend the written word.

ACKNOWLEDGEMENTS

Education is a guided journey. Research is intrinsically collaborative. The work of this master's thesis encompasses both. Without the support of certain entities and individuals, I would still be in the lab collecting data, searching for the light at the end of a few tunnels.

My sincere thanks to Mr. Tom Barclift and Esstech, Inc. of Essington, Pennsylvania. Their generous donations of materials, on multiple occasions, allowed me to conduct and complete my research. To Mr. Gary Fleener and the gentlemen at the Professor Edward J. Blair Mechanical Instrument Services of the Indiana University Chemistry Machine Shop in Bloomington, Indiana. Their generous donation of time and labor in fabricating the single aperture masks were the core of my project. When all options seemed exhausted, they stepped forward after a single e-mail to help me because "we're here for the students, all you IU Hoosiers, regardless which campus you study."

I would also like to thank both the Indiana University School of Dentistry and Indiana University-Purdue University Indianapolis, for the opportunity to pursue my graduate degree while serving as a full-time employee through the Tuition Benefit Program.

Gratitude is also owed to the members of my thesis committee. Drs. Brown and Naumann, thank you for your time and guidance over the course of both my graduate program and my thesis research.

Dr. Moore, I am quite certain "retirement" is not a word in your vocabulary. They just don't make engineers and educators like they used to, and I am deeply honored

to have had the opportunity to learn from you both in and out of the lab. You were always willing to lend me a hand without hesitation, be it for work or my research. It also doesn't hurt that I could share "war" stories about my lab battle scars with the reigning champion.

Dr. Platt, you are bar none one of the finest educators and mentors I have had the privilege of learning from. You are also quite a gambler, hiring me with the knowledge that I was quite set on pursuing a master's degree on a part-time basis. I'm confident neither of us realized at the time you'd be serving as both my supervisor and professor, but I'm more confident no one else could have done a finer job. Without your willingness to gamble, this degree would have never gotten off the ground. It is the lessons applicable to life outside the lab or classroom, however, which I am most grateful for.

Dr. Chu, chair of my thesis committee, thank you for providing me with a project that was challenging on so many levels. I must confess, at that first meeting nearly two years ago when you introduced me to the project, I thought you were out of your mind. I remember vividly your second sentence of that conversation, "Meoghan, there's a good chance it won't work. At all." For quite some time, I couldn't understand why you selected this project for me, but I do now. You always treated me as a colleague, providing guidance, supporting my insights and ideas, and even sharing a few "high fives" along the way. Your course lectures were delivered with passion, excitement, and humor. I was constantly reminded throughout this process how much fun engineers could have, and how rewarding hard work can be even when the data is less than desirable. You also instilled upon me the importance of finding balance in life, making

time for one's professional life, intellectual pursuits, and family. Working under your wing has been an absolute privilege.

To Ghaeth and Laila, my dear friends and classmates. Whether you were helping me to overcome obstacles with an experiment, asking if there was anything you could do to help me with my research, or genuinely asking me how I was while sternly reminding me to get enough sleep, you two kept me going. Without you, I am quite certain I would have pulled all of my hair out and been severely sleep deprived. There really aren't enough words.

To Ms. Jeana Aranjo, when I just needed an ear to listen, you were always there. Monday mornings were so much easier after a long weekend of time in the lab thanks to you; sharing a cup of coffee and checking in on how thing were going even if you had not a clue what I was talking about. You did it with a smile, comforting nod, and sometimes a laugh.

Last but not least, I am and will always be grateful for my family. I am blessed to have parents who have fostered and encouraged my love of science and the unique, parents who also firmly believe in the importance of education. From my younger days of collecting bugs and summer science camps, to my pursuit of an engineering degree and this master's degree in Dental Materials, you never said "no." I am equally blessed with two younger brothers, Michael and David, who have always stood by my side, defended my uniqueness, and somehow knew just when to call with words of encouragement or with some ridiculous comment for a good laugh. On many occasions you've told me you don't always understand what I do, but because it makes me happy you are all for it. What more could a big sister ask for.

TABLE OF CONTENTS

LIST OF TABLES viii

LIST OF FIGURES ix

INTRODUCTION 1

EXPERIMENTAL PROCEDURES 10

Materials 10

Methods: Curing Profile Under a Point Light Source 12

Methods: Effect of a Point Light Source on Polymerization 17

Statistical Analysis 23

RESULTS 25

DISCUSSION AND FUTURE DIRECTIONS 30

TABLES 34

FIGURES 47

REFERENCES 79

CURRICULUM VITAE

LIST OF TABLES

Table 1: Composition of the model resin composite 34

Table 2: Drill bit and aperture details 34

Table 3: Mean(SD) bullet width and depth..... 35

Table 4: Semi-major and semi-minor values 36

Table 5: D_p and E_c values 37

Table 6: D_p' and E_c' values..... 37

Table 7: Cure depth values (b) derived from mathematical models 38

Table 8: Bullet radius values (a) derived from mathematical models 39

Table 9: Curing protocols and top surface energy 40

Table 10: Mean(SD) top, bottom, and B/T degree of conversion 41

Table 11: Comparison of top degrees of conversion between modes 42

Table 12: Comparison of bottom degrees of conversion between modes 42

Table 13: Comparison of B/T degree of conversion ratios between modes 43

Table 14: Mean(SD) top surface Knoop hardness numbers 44

Table 15: Comparison of Knoop hardness numbers between modes 45

Table 16: Mean(SD) polymerization shrinkage stress at 30 minutes 46

Table 17: Comparison of the control group polymerization shrinkage stresses 46

LIST OF FIGURES

Figure 1: Predicted curing phenomenon beneath a point light source 47

Figure 2: Single aperture masks 47

Figure 3: QHL75 spectral range and irradiance 48

Figure 4: Experimental setup to investigate point light source curing 49

Figure 5: Stages of exposing the cured resin bullet 49

Figure 6: Measurescope and digital readout system 50

Figure 7: PocketGoniometer 51

Figure 8: FTIR 52

Figure 9: Representative degree of conversion curves 53

Figure 10: Knoop hardness tester 54

Figure 11: ADA tensometer 55

Figure 12: Representative shrinkage stress vs. time curves 56

Figure 13: Experimental setup for side curing 57

Figure 14: Representative side profile images of cured resin bullets 58

Figure 15: Linear regression analysis of width vs. time 59

Figure 16: Linear regression analysis of cure depth vs. time 59

Figure 17: 0.5 mm mask x-y scatter plots 60

Figure 18: 0.4 mm mask x-y scatter plots 61

Figure 19: 0.25 mm mask x-y scatter plots 62

Figure 20: Scatter plots of investigated SAM-cure time combinations 63

Figure 21: Non-linear regression analysis of bullet width vs. energy 64

Figure 22: Non-linear regression analysis of bullet cure depth vs. energy 64

Figure 23: 0.5 mm, 10 second model scatter plot-side profile overlay..... 65

Figure 24: 0.4 mm, 10 second model scatter plot-side profile overlay..... 66

Figure 25: 0.25 mm, 30 second model scatter plot-side profile overlay..... 67

Figure 26: 0.25 mm, 40 second model scatter plot-side profile overlay..... 68

Figure 27: Standard mode mean top degree of conversions..... 69

Figure 28: Standard mode mean bottom degree of conversions..... 70

Figure 29: Standard mode mean bottom/top degree of conversion ratios 71

Figure 30: Plus mode mean top degree of conversions 72

Figure 31: Plus mode mean bottom degree of conversions 73

Figure 32: Plus mode mean bottom/top degree of conversion ratios..... 74

Figure 33: Standard mode mean Knoop hardness numbers..... 75

Figure 34: Plus mode mean Knoop hardness numbers..... 76

Figure 35: Standard mode mean shrinkage stresses at 30 minutes..... 77

Figure 36: Plus mode mean shrinkage stresses at 30 minutes 78

INTRODUCTION

Polymerization Shrinkage Stress

Investigation of dimethacrylate-based resin composites, their polymerization, and the resulting shrinkage stresses is hardly a contemporary discipline. In 1967, the work of Dr. Rafael L. Bowen introduced the phenomenon of "hardening shrinkage" of those composite materials bonded to solid tooth structure of a cavity wall [1]. Through his continued work and that of his colleagues, the early 1980s was marked by a surge of interest in the area of polymerization shrinkage stress and its reduction, most notably by Davidson, De Gee, and Feilzer [2-5]. Nearly fifty years later, polymerization shrinkage stress remains a compromising factor in the success of photopolymerized, dimethacrylate-based dental composites.

Photopolymerization of a dental resin composite is the chemical reaction that transforms small molecules into large polymer chains or networks; it is a complex and fast reaction transforming a viscous-plastic into a rigid-elastic phase [6]. Photoinitiators are activated by a light source, and converted to an excited state in which they are able to react with a coinitiator to form free radicals. These free radicals in turn react with monomer molecules to create an active center and the polymerization process propagates. The polymer chain grows by rapid, sequential addition of monomer to the active centers through covalent bonds until the maximum conversion of carbon-carbon double bonds into carbon-carbon single bonds is achieved [7,8]. Conversion of the monomer molecules into a polymer network is associated with closer packing of the molecules resulting from the reduction of the intermolecular distance between monomeric units. Prior to polymerization, monomer molecules are at intermolecular distances of 3-4 Å, but after

polymerization distance between the polymer units is only 1.5 Å [9-11]. This reduction of intermolecular distances leads to a bulk volumetric contraction of the resin composite typically in the order of 1-5% [8,12,13].

Polymerization shrinkage stress is the product of this volumetric contraction taking place under confinement, due to bonding of the resin composite to the cavity walls [14,15]. The stresses result from the rigid nature of the reinforced cross-linked polymer network formed during the course of the polymerization reaction [8]. These stresses, however, challenge the integrity of the resin's bond to tooth structure.

If the polymerization shrinkage stress exceeds either the adhesive or cohesive strength of the system, micro- or macro- defects can result [16]. In areas where the shrinkage forces exceed the bonding strength at the interface, a gap will develop, resulting in the incomplete sealing of the tooth-restoration interface and increasing the possibility of post-operative sensitivity and pain, marginal staining, bacterial microleakage, and recurring caries [17-22]. Should this interface be preserved, however, the contraction forces can be transferred to neighboring dental structures leading to cuspal deflection or cracks in the enamel [7,11,23,24]. A well-preserved interfacial bond between the resin composite and tooth structure as well as maintenance of the surrounding dental structure is of vital importance to the success of a composite restoration [19]. Efforts to reduce polymerization shrinkage stress and thereby enhance the clinical performance of composite restorations have taken one of two approaches: modification of the material or modification of the curing scheme.

Materials Approach to Reducing Shrinkage Stress

The inclusion of nanofillers (fibers and spheres) in modern dental resin composites provides a large surface area to volume ratio, increasing the possibility of surface reaction between filler and polymerizing monomer and thereby increasing the potential for stress through constraint of molecule mobility during polymerization [8]. One potential solution to relieve polymerization shrinkage stress would be the inclusion of non-surface treated silica nanofillers and polyethylene spheres, or those treated with a non-functional silane coupling agent. Such fillers would minimize the interaction between the developing polymer and the filler surface [8,18]. Non-bonded micro- and nano-fillers have also been introduced to achieve controlled pore structure, as microscopic porosity in the resin composite prior to polymerization results in reduced polymerization shrinkage and stress development as a result of the formation of enlarged voids in the polymer [16]. Incorporation of ultrahigh molecular weight polyethylene fibers, whose intrinsic properties allow for plastic deformation as polymerization shrinkage stress develops, could also reduce the overall contraction stress of the system [7].

The typical dimethacylate monomers used in modern dental composites can also be replaced with alternative monomers. New silorane and oxirane (cycloalipathic epoxy resin) chemistries provide for a reduction in shrinkage stress while maintaining comparable properties to methacrylate based resin composites of similar cross-link density [8,16,18]. Instead of free radical polymerization of the dimethacrylate monomers, siloranes are dependent upon ring opening polymerization of the silorane molecules. These monomers open their molecular structures with local volumetric expansion, which compensates for the volumetric shrinkage from carbon-carbon double bonds [7]. Ordered

liquid crystalline monomers yielding amorphous polymers have also been developed [16]. Development of low-shrinkage monomers and novel filler-monomer systems that match clinically important properties of current dimethacrylate based resins however, is a challenging task.

Curing Protocol Approach to Reducing Shrinkage Stress

Several modifications to the curing scheme have been investigated in the literature. These "soft-start" methods are the two-step, pulse-delay, and ramped curing modes. In the two-step method, an initial exposure of reduced intensity is applied for a short period of time and then immediately followed by an exposure of higher intensity for the final cure of the resin composite [7,15,21,25,26]. The pulse-delay method also involves an initial application of lower intensity exposure followed by a final cure at a higher intensity, but there is a waiting or dark period without irradiance between these two applications [7,15,21,25,26]. In the ramped curing mode, irradiance is gradually increased over the course of the exposure stepwise, linearly, or exponentially [21,26].

Theoretically, polymers cured at slower rates allow more time for viscous flow and polymer chain relaxation prior to reaching the gel point [8,9,17,27]. This slower rate delays the onset of polymerization shrinkage stress, extending the pre-gel phase where shrinkage forces can be dissipated before polymer cross-linking reaches an advanced stage of vitrification, after which compensation of the stress is severely hindered [12-14,26-29]. Therefore, the greater proportion of the total volumetric shrinkage occurring while the resin composite remains in a non-rigid state leaves a smaller fraction of the shrinkage available to contribute to stress development [18]. Soft-start modes of polymerization with

initial light exposures at lower irradiance levels could lead to the formation of fewer polymer growth centers, slow the reaction rate, delay and decrease stress development, and thereby reduce damage at the adhesive interface [7,11,23]. There are mixed reviews in the literature, however, on the success of these methods to reduce shrinkage stress and their ability to do so without negatively impacting the degree of conversion and mechanical properties of the restoration.

For as many studies which conclude that a significant reduction in shrinkage stress using soft-start polymerization occurs at no expense to the degree of conversion and mechanical properties, there are those having observed a significant decrease in final conversion [15,17,22]. It has also been demonstrated that a soft-start polymerization provides no additional advantages in the reduction of polymerization shrinkage stress [9]. With specific regards to the pulse-delay method, in order for adequate shrinkage stress relaxation to be achieved, a clinically impractical relaxation time between the two irradiances is necessary [11,15,19]. Concerns have also been raised with respect to the integrity of the final polymer structure. Despite equivalent degrees of conversion, it is possible that the soft-start methods will lead to different polymer structures. Fewer centers of polymer growth may result in a more linear polymer structure with relatively few crosslinks and therefore more likely to be influenced by softening substances of food or by enzymatic attack [25]. A more linear polymer structure could also result in an increased release of residual free monomer, compromising the health of surrounding oral tissues. The effectiveness of different soft-start protocols may also be influenced by material composition; thereby making the development of a universal protocol producing

a significant reduction of shrinkage stress for the majority of commercial composites a challenging task. Such a challenge requires an innovative approach.

Photopolymerization Through Single Apertures

The soft-start methods of polymerization combine low intensity light with exposures of high intensity light, in efforts to cure resin composites with reduced polymerization shrinkage stress. When using these methods, the gel point of the overall polymer structure, while delayed, occurs at once. According to the Carothers theory of gelation, polymers have the ability to form infinite networks (the gel point) at relatively low levels of conversion [30]. Remaining unreacted functional groups of the polymer structure are able to contribute to the shrinkage stress of the resin composite as final stages of polymerization commence. By the Carothers theory, approximately 50% or more of the functional groups remain unreacted at the gel point. If we can polymerize the polymer network to a higher degree of conversion prior to the gelation of the overall structure, we can potentially further reduce the polymerization shrinkage stress. It is our prediction that this is possible through the use of a point light source.

By photo-curing through a single aperture mask, a dental light curing unit is transformed from a planar light source to a point light source. A fully cured, three-dimensional bullet shaped curing front is predicted for the resin beneath the aperture. The surface profile, its curing front, defines the most exterior surface where the polymer network can gel and form an insoluble cross-linked structure. The bullet can be cured to a final degree of conversion and will generate shrinkage stress within itself, but so long as the edges and curing front do not touch the cavity walls or floor, the shrinkage stress of

the bullet is not transferred across the restoration; the bullet's shrinkage stress is able to relax within the uncured polymer network (Figure 1). The source of polymerization shrinkage stress for the overall polymer structure is the uncured resin separating the bullet from the cavity walls and floor. This phenomenon has significant implications as a potentially novel method for reducing the polymerization shrinkage stress of dental resin composites.

We propose that conversion of the overall polymer structure can be maximized, while the volume of uncured polymer sufficient to isolate the bullet minimized. By reducing the volume of uncured composite in contact with the cavity walls and floor, shrinkage stress of the restoration is also reduced. Follow-up with a planar light source, an unmasked light curing unit, fully polymerizes the restoration. To quantitatively describe the curing front and predict the size of the three-dimensional bullet, we utilize mathematical modeling.

Mathematical Models in the Literature

Several models have been proposed to describe the relationship between the depth of cure and exposure, and between the depth of cure and curing time of photopolymerized dental resin composites [31-40]. Using infrared spectroscopy to determine monomer conversion, Rueggeberg et al., studied the significance of time, intensity, filler type, and shade on the polymerization of resin composites [34]. Their experimental results generated a predictive mathematical model for the extent of resin composite polymerization. Standardizing variables such as light source, filler type, and filler surface treatment, Emami et al. investigated the potential prediction of light

absorption in photopolymerized resin composites with respect to Beer-Lambert's law [36]. Despite its complexity, their mathematical model allowed them to determine how such variables affect light attenuation and revealed significant differences in adsorption values for different materials. Chen et al. utilized a Monte Carlo model to simulate photon migration within resin composite materials to predict absorbed radiant exposure distribution, and thereby determine the light-curing efficiency for a photopolymerized system [37]. Their overlying goal was to develop a simple model based on reciprocity of irradiance and exposure time which accurately predicts the depth of cure for any resin composite. The relationships and models presented by these works, however, only describe the curing behavior underneath the surface of an uncured composite polymerized by a planar light source, a dental light curing unit.

In 1992, Jacobs proposed a simple mathematical model describing the depth of cure and curing energy in unfilled photopolymers cured with a linear light source [41]. Jacobs' model describes a linear relationship between the depth of cure of a composite resin and the natural logarithm of the energy applied to the surface of the resin. Specifically:

$$C_d = D_p \ln\left(\frac{E}{E_c}\right)$$

where C_d is the cure depth of the composite resin, E is the energy applied to the surface of the resin, E_c is the critical energy required to reach gel point, and D_p is the characteristic penetration depth where the energy is reduced to 1/e of E. Several years later, Chu et al. demonstrated that this relationship also held for particle-filled polymer slurries [42]. When a liner light source is used, a laser beam traveling across the surface of the resin composite for example, a two-dimensional curing front develops underneath the

composite taking a parabolic shape [41]. A similar phenomenon was demonstrated by Chen et al., as the two-dimensional cross section of radiant exposure underneath the surface revealed a hemi-elliptical curing front [37]. From these models, it can be predicted that when a point light source is used, a three-dimensional bullet-shaped curing front will develop underneath the surface of a resin composite.

Specific Aims

The overall objective of this study was to investigate the curing phenomenon under a single point light source and its effects on the polymerization of a model resin composite. To accomplish this, the specific aims were:

1. To demonstrate and mathematically model the curing phenomenon of a model resin composite polymerized under a point light source.
2. To evaluate the effect of point light source polymerization on the degree of conversion of a model resin composite.
3. To evaluate the effect of point light source polymerization on the Knoop hardness of a model resin composite.
4. To evaluate the effect of point light source polymerization on the polymerization shrinkage stress of a model resin composite.

The null hypothesis of this study was that point light source polymerization would not significantly increase the degree of conversion and Knoop hardness, nor significantly decrease the polymerization shrinkage stress of a model resin composite.

EXPERIMENTAL PROCEDURES

Materials

Model Resin Composite

Chemical Composition and Ratios

A 1:1:1 weight ratio mixture of bisphenol A-glycidyl methacrylate (Bis-GMA), urethane dimethacrylate (UDMA), and triethylene glycol dimethacrylate (TEGDMA) (Esstech, Inc., Essington, PA) served as the neat resin base for the methacrylate based model resin composite (MRC). The addition of camphorquinone (CQ) (Esstech, Inc.), dimethylaminoethyl methacrylate (DMAEMA), and butylhydroxytoluene (BHT) (Sigma-Aldrich, St. Louis, MO) in weight percentages of 0.5%, 0.25%, and 0.5%, respectively, completed the matrix phase. The filler was a 30% BaO, silanated, barium borosilicate dental glass (BBAS) (Esstech, Inc.) having a mean particle size of 0.7 μm (Table 1).

Composition of the final MRC was 30% matrix phase and 70% BBAS filler by weight.

Preparation

A 50:50 Bis-GMA:TEGDMA stock solution was received from Esstech, Inc. This solution was mixed with UDMA in a wide-mouth jar under continuous stirring to make a 1:1:1 ratio neat resin. To ensure homogeneity, this was left to mix on a magnetic stir plate set at a medium-low speed. After 24 hours of continuous stirring, the neat resin was placed under vacuum for 24 hours to extract any air bubbles and stored at 5° C until desired use. The monomers were used as received without purification.

Under dark conditions, CQ, BHT, and DMAEMA were mixed with a metal spatula in a wide-mouth amber jar until the CQ and BHT were completely dissolved in the DMAEMA. After dissolution, the neat resin was added from the stock directly to the amber jar. This matrix phase was left to stir under dark conditions on a magnetic stir plate set at a medium-low speed to ensure homogeneity. After 24 hours of continuous stirring, the matrix phase was placed under vacuum for 24 hours to extract any air bubbles.

BBAS filler was incorporated by hand into the matrix phase. After thorough mixing, the finished MRC was placed under vacuum for 24 hours to extract any air bubbles which may have resulted from the manual mixing. During the course of the study, the MRC was stored at 5° C.

Single Aperture Masks and the Light Curing Unit

Fabrication of the Masks

Single aperture masks (SAMs) were fabricated by first cutting 0.4 mm thick disks from machined aluminum rod (ø=13 mm) using an Isomet 1000 Precision Saw (Buehler, Lake Bluff, IL). Next, a single aperture was created in the center by drilling through the disk with a standard drill bit. After drilling, the masks were lightly finished on both sides with wet 600 grit SiC paper. For the purposes of this study, three aperture diameters were selected: 0.5 mm, 0.4 mm, and 0.25 mm (Table 2, Figure 2).

Selection and Characterization of the Light Curing Unit

Based on previous pilot work, the QHL75 light curing unit (Dentsply, York, PA) with an 8 mm diameter curing tip was selected for the study. Spectral characteristics

(average irradiance and spectral range) of this halogen light curing unit were determined using a MARC® Resin Calibrator (BlueLight Analytics, Inc., Halifax, NS, Canada). The MARC® Resin Calibrator incorporates a laboratory grade UV-VIS spectrometer and two (top and bottom) laboratory grade cosine corrected sensors. Light captured by the sensors is transmitted to the spectrometer through a bifurcated fiber optic cable, after which dedicated software provides real-time irradiance data display.

Spectral characteristics were collected by placing the curing tip flush against the surface of the top cosine corrected sensor. Setting the MARC® Resin Calibrator to monitor the QHL75 for 60 s, irradiance was continuously measured for 60 s and an average irradiance calculated. The light's spectral range was also measured and displayed graphically. Irradiance and spectral range were monitored for five trials (Figure 3). The average irradiance for the QHL75 light curing unit was determined to be 748 mW/cm^2.

Methods: Curing Profile Under a Point Light Source

Demonstration of the Curing Phenomenon Under a Point Light Source

Specimen Preparation and Exposure of the Curing Front

Under dark conditions, a clean glass slab was placed on sheet of brown bench paper. Next, a Delrin® mold (h=5 mm, ID=6 mm) was placed on the clean glass slab and slightly overfilled with the MRC. A 1 mm thick glass microscope slide was then placed over the resin filled mold and sufficient pressure applied (100 g balance calibration weight, 20 s) to remove excess material and prevent entrapment of air bubbles. Next, a SAM was placed over the glass slide and positioned such that the aperture of the mask

aligned with the center of the resin filled mold (Figure 4). The specimen was cured, after which the SAM was removed.

Following removal of the SAM, the resin filled mold and glass slide were gently separated from the lower glass slab and laid to rest (glass slide facing down) on the lab bench. To expose the curing front, alternating applications of a gentle acetone wash and compressed air were applied until only cured resin remained within the mold. The Delrin® mold was removed from the glass slab with a sharp scalpel, and a final application of acetone wash and compressed air applied to the cured resin before being placed overnight in a desiccator (Figure 5).

For each of the three SAMs, curing times of 10, 20, 30, and 40 s were investigated. Five specimens for each SAM-cure time combination were fabricated.

Measurement of Select Bullet Dimensions

Based upon the dome-shaped, bullet-like appearance of the cured resin profiles the dimensions of width (diameter) and cure depth (height) were measured.

To measure bullet width, a specimen was secured (flat side down) to a glass microscope slide with double-sided tape. The slide was placed on the stage of a UM-2 Measurescope (Nikon Metrology, Inc., Brighton, MI), and the diameter of the bullet measured with a ND1200 Quadra-Check digital readout system (Heidenhain, Schaumburg, IL) (Figure 6). The bullet was rotated 120° and a second measurement taken. A third measurement was made in the same manner and an average width calculated.

To measure cure depth, a glass microscope slide was secured to a Teflon® block. A specimen was secured (flat side down) to the glass slide with double-sided tape, and

the Teflon®-slide-bullet assembly placed on the stage of the measurescope. The Teflon®-slide-bullet assembly was rotated 90° on its side such that when looking through the eyepiece, the bullet's dome-shaped profile was in the field of view. The cure depth of the bullet was measured with the digital readout system, the bullet rotated 120°, and a second measurement taken. A third measurement was made in the same manner and an average cure depth calculated.

Imaging the 3D Bullets

To evaluate the curing phenomenon qualitatively, side profiles of the bullets were photographed. Utilizing the camera feature of the PG-2 PocketGoniometer (Testing Machines, Inc., New Castle, DE), each bullet was centrally placed on the stage of the goniometer and an image of the semi-circular side profile captured (Figure 7). One picture of each specimen was taken.

Theoretical Modeling of the Curing Phenomenon Under a Point Light Source

Modeling the 2D Curing Front Profile

As previously mentioned, the curing front profile of the bullets was dome-shaped. Based on this observation, an ellipsoid dome was selected to model the 2D curing fronts. A horizontal ellipse whose major axis and minor axis coincide with the axes of the Cartesian coordinate system is mathematically defined as follows:

$$\frac{x^2}{a^2} + \frac{y^2}{b^2} = 1$$

Where the semi-major axis of the ellipse (equal to one half of the diameter) is *a*, and *b* is the semi-minor axis (equal to the height). For the cured resin bullets, *a* is equal to one half of the mean width and *b* is the mean cure depth. Rearranging this equation into "y -

equals form", yields:

$$y = \sqrt{b^2 - \frac{b^2 x^2}{a^2}}$$

In the case of an ellipsoid dome, the *x* and *y* values are limited by the conditions of:

$$-a \leq x \leq a \text{ and } 0 \leq y \leq b$$

To model the 2D curing front profiles, for each SAM-cure time combination the corresponding values of *a* and *b* were substituted into the rearranged equation for an ellipse. Using this SAM-cure time specific equation, values of *x* at the extremes and within the limiting conditions stated above were substituted into the equation in refined increments of 0.1mm to solve for *y*. The resulting *x,y* coordinate pairs were then plotted in Microsoft® Excel 2010 as an x-y scatter plot.

Prediction Modeling of the 2D Curing Front Profile

Although the ellipsoid dome approach does characterize the curing front profile of the cured resin bullets, it is dependent upon the measured *a* and *b* values of a specimen for a given SAM-cure time combination. Such methodology is impractical for the investigation of a wide range of curing times, and therefore unsuccessful in providing a more comprehensive model of the curing front profile. In an effort to correct this deficiency, a prediction model of the curing front profile was evaluated.

Jacobs' derivation of the relationship between cure depth and energy describes a linear relationship between the depth of cure of a composite resin and the natural logarithm of the energy applied to the surface of the resin. Specifically:

$$C_d = D_p \ln\left(\frac{E}{E_c}\right)$$

where C_d is the cure depth of the composite resin, E is the energy applied to the surface of the resin, E_c is the critical energy required to reach gel point, and D_p is the characteristic penetration depth where the energy is reduced to 1/e of E. Recognizing C_d as *b* from our ellipsoid dome model, a simple substitution approach was taken for the derivation of the prediction model.

To account for *a*, the parameter C_w was identified as the width counterpart of C_d to describe the lateral spreading of the composite resin. As such, C_w was defined as:

$$C_w = D_p' \ln\left(\frac{E}{E_c'}\right)$$

where D_p' and E_c' are the lateral cure distance and critical energy specific to the width of the cured resin bullet. Since *a* represents the radius of the bullet, ½ of C_w is its equivalent.

Substituting C_d and ½ C_w into the "y-equals" form of our ellipsoid dome formula, the resulting prediction model for the curing front profile is:

$$y = \sqrt{\left[D_p \ln\left(\frac{E}{E_c}\right)\right]^2 - \frac{\left[D_p \ln\left(\frac{E}{E_c}\right)\right]^2 x^2}{\frac{1}{2}\left[D_p' \ln\left(\frac{E}{E_c'}\right)\right]^2}}$$

With the limiting conditions of:

$$-\frac{1}{2}\left[D_p' \ln\left(\frac{E}{E_c'}\right)\right] \le x \le \frac{1}{2}\left[D_p' \ln\left(\frac{E}{E_c'}\right)\right]$$

and

$$0 \le y \le D_p \ln\left(\frac{E}{E_c}\right)$$

The values of D_p, E_c, D_p', and E_c' were calculated from non-linear regressions of the bullet width and bullet cure depth v energy (logarithmic scale) data for each SAM.

To evaluate the prediction model of the curing front, an x-y scatter plot was constructed in Microsoft® Excel 2010 for each SAM-cure time combination in an identical manner to the previously described method.

Methods: Effect of a Point Light Source on Polymerization

Definition of Curing Protocols and Identification of Experimental Groups

Curing Protocols

For all experimental procedures, a 60 second curing time without a SAM served as the control group.

The **standard mode** of polymerization was defined by a total curing time of 60 s, whereby an initial cure with a SAM was immediately followed with curing without the SAM:

Total Curing Time (60 s) = Initial Cure w/ SAM + Follow-Up Cure w/o SAM

In this mode of polymerization, total energy applied to the top surface of a specimen varied among experimental groups, but the total curing time remained the same.

The **plus mode** of polymerization was defined by an initial cure with a SAM immediately followed by 60 s of curing without the SAM:

Total Curing Time (+60 s) = Initial Cure w/ SAM + Follow-Up Cure w/o SAM (60 s)

In this mode of polymerization, the total energy applied to the top surface of a specimen was held relatively constant (equal to the curing energy of the initial cure plus the energy applied to the top surface during the follow-up cure). This was done to ensure sufficient curing.

Experimental Groups

SAM-cure time combinations for the initial cure component of the experimental groups were limited by the polymerization shrinkage stress testing configuration's height component (methodology to follow). To ensure that the outer edges of the resin bullets did not touch the quartz rods, only those SAM-cure time combinations yielding a bullet diameter less than 3 mm were investigated.

The Effect of a Point Light Source on the Degree of Conversion

Background

In this infrared spectroscopic technique, the degree of conversion (DC) of a resin composite is measured with a Fourier transform infrared spectrometer (FTIR) in attenuated total reflection (ATR) mode (FT/IR-4100, JASCO Analytical Instruments, Easton, MD) (Figure 8). The degree of conversion is calculated utilizing the mid-IR range peaks of 1608 cm^{-1} and 1638 cm^{-1} (Figure 9). The area under the peak at 1638 cm^{-1} (P1) represents the vinyl C=C groups of the resin composite, while the area under the peak at 1608 cm^{-1} (P2) represents the aromatic C=C and serves as the internal standard. DC is calculated directly from an intensity decrease at 1638 cm^{-1} using the following equation:

$$\mathrm{DC} = \left(1 - \left(\frac{cured\ \left(\frac{P1}{P2}\right)}{uncured\ \left(\frac{P1}{P2}\right)}\right)\right) \times 100\%$$

Specimen Fabrication

Under dark conditions, a clean glass slab was placed on sheet of brown bench paper. Next, the glass slab was lined with Mylar®. A clear plastic tube (h=6 mm,

ID=6.35 mm) was placed on the Mylar® lined, clean glass slab and slightly overfilled with the MRC. A Mylar® square was then placed over the resin filled mold, followed by a 1 mm thick glass microscope slide. Sufficient pressure was applied (100 g balance calibration weight, 20 s) to remove excess material and prevent entrapment of air bubbles. The glass slide was removed and a SAM placed over the Mylar® square, positioned such that the aperture of the mask aligned with the center of the resin filled mold. The specimen was then polymerized according to the curing protocol of its respective group. Five specimens for each group were fabricated.

After polymerization, the top and bottom surfaces of a specimen were polished with wet 600 grit SiC paper before 0.4 mm "thin" slices were sectioned from the top and bottom of the specimen with an Isomet 1000 Precision Saw. Each top-bottom pair of "thin" slices was ultrasonically cleaned for 6 minutes in Type I DI H_2O, blotted dry with a Kimwipe™, and further dried with compressed air.

Measurement of the Degree of Conversion

For the uncured MRC, a small quantity of the MRC was placed directly on the spectrometer's ZnSe crystal (ø =1.8 mm) under dark conditions (Figure 8). Spectra were collected in absorbance mode between wavenumbers of 1500 cm^{-1} and 1700 cm^{-1}, from 64 coadded scans at a wavenumber resolution of 4 cm^{-1}. Three scans of the uncured MRC were performed.

For the cured MRC, a "thin" slice was placed directly on the spectrometer's ZnSe crystal sample holder with the surface of interest facing the crystal (upper surface of the top "thin" slice and lower surface of the bottom "thin" slice). Spectra were collected in

the same manner as for the uncured MRC. Three scans from different areas of the surface (left, center, and right) for each slice were performed.

Each spectrum was processed with smoothing and baseline correction.

The Effect of a Point Light Source on the Knoop Hardness

Background

A micro-hardness test, Knoop hardness is a measure of a material's ability to be plastically deformed by indentation; a higher Knoop hardness number (KHN) reflects a harder material. A pyramidal diamond indenter is applied to the flat, polished surface of a test material for a specified dwell time with a known force, and the resulting indentation is measured using a microscope. The KHN is the ratio of the applied load to the area of the resulting indentation using the following equation:

$$\mathrm{KHN} = \frac{P}{\mathrm{C_p L^2}}$$

where P is the applied load (kgf), C_p is a constant relating L to the projected area of the indentation, and L is the length of the indentation along its long axis (mm). The units for KHN are kg/mm^2.

Specimen Fabrication

Under dark conditions, a clean glass slab was placed on sheet of brown bench paper. Next, the glass slab was lined with Mylar®. A clear plastic tube (h=6 mm, ID=6.35 mm) was placed on the Mylar® lined, clean glass slab and slightly overfilled with the MRC. A Mylar® square was then placed over the resin filled mold, followed by a 1 mm thick glass microscope slide. Sufficient pressure was applied (100 g balance calibration weight, 20 s) to remove excess material and prevent entrapment of air

bubbles. The glass slide was removed and a SAM placed over the Mylar® square, positioned such that the aperture of the mask aligned with the center of the resin filled mold. The specimen was then polymerized according to the curing protocol of its respective group. Five specimens for each group were fabricated.

After polymerization, the specimens were cross-sectioned with an Isomet 1000 Precision Saw and top halves set-aside. The upper surface of these top samples were polished with wet 400, 600, 800, and 1200 grit SiC paper sequentially. The samples were then ultrasonically cleaned for 6minutes in Type I DI H_2O, blotted dry with a Kimwipe™, and further dried with compressed air.

Measurement of the Knoop Hardness

Top half samples were placed on the loading platform of an M-400 Hardness Tester (LECO, St. Joseph, MI) (Figure 10). Under an applied load of 50 g with a dwell time of 15 s, an indentation was made on the top surface with the diamond Knoop indenter. The length of the indentation was then measured optically at 20x magnification, and a KHN calculated automatically by the hardness tester. Three indentations, at least 1 mm apart were made for each top half sample.

The Effect of a Point Light Source on the Polymerization Shrinkage Stress

Background

A tensometer (ADA Foundation/Paffenbarger Research Center, Gaithersburg, MD) is a variable tension load cell whose operation is based upon basic engineering beam theory (Figure 11). When a tensile load generated by a shrinking resin composite specimen pulls down upon a cantilevered beam (stainless steel rectangular beam, 10 mm

in width and 40 mm in height; Young's modulus of 193 GPa), the load causes the beam to bend downward. This downward bending is measured with a linear variable differential transformer (LVDT) located 23 cm away from the sample assembly at the free end of the cantilever beam.

The load (tensile force) is calculated based upon the beam's calibration constant, which is depended upon the distance between the specimen position on the beam and the start of the cantilever. Polymerization shrinkage stress (PSS) is then calculated by dividing the measured tensile force by the specimen's cross-sectional area and reported in MPa (Figure 12).

Specimen Fabrication

Two vertically positioned quartz rods (ø=6 mm) and a clear plastic tube (L=13 mm, ID=6.35 mm, and a wall thickness=0.79 mm) formed the sample holder: an upper rod connected to the cantilever beam 12.50 cm from the beam holder, a lower rod, and the plastic tube to hold the resin composite in place (Figure 11). To prepare the quartz rods, the ends were cut with the Isomet 1000 Precision Saw, polished with wet 600 grit SiC paper, and twice silanated with Lute-It Silane Coupler (Pentron Clinical, Orange, CA). Two holes were drilled into opposing sides of the plastic tube: one for sample injection and the second for the extrusion of air and excess material.

To better mimic the clinical situation, a side curing (as opposed to bottom-up) test setup was selected. In this orientation, the direction of the polymerization shrinkage stress is perpendicular to the light source. Using a gauge block, the distance between the quartz rods was fixed at 3 mm. Next, the SAM was secured against the side of the acrylic tube and held in position using black electrical tape and a plastic spatula (Figure 13). The

aperture of the SAM was then centered relative to the ends of the upper and lower quartz rods to ensure the edges of the cured bullets would not contact the rods during formation. Under dark conditions, MRC was injected into the sample holder to completely fill the space. The specimen was then polymerized from the side of the specimen holder assembly according to the curing protocol of its respective group.

Measurement of the Polymerization Shrinkage Stress

Polymerization shrinkage stress was measured for 30 minutes from the start of polymerization, with data collected every second. Five specimens for each group were tested.

Statistical Analysis

Summary statistics (mean and standard deviation) for bullet width and cure depth were calculated for each SAM-cure time combination. Analysis of the measured and prediction curing front profile models was conducted by overlaying the bullet side profile images with the respective x-y scatter plot for each SAM-cure time combination. To compare the two models, a prediction error was calculated for each SAM-cure time combination.

Summary statistics for top and bottom degree of conversion were calculated for each group. Bottom-top degree of conversion ratios (B/T) were also computed for each specimen and B/T summary statistics calculated for each group. Summary statistics for top surface Knoop hardness and maximum PSS at t_{30mins} were calculated for each group.

Group differences were analyzed using a one-way ANOVA at a 5% significance level (α=0.05). Because of non-homogeneous variances, each group combination was

allowed to have a different variance in the ANOVA. Pair-wise comparisons were performed using a simulation-based method.

RESULTS

Demonstration of the Curing Phenomenon

Summary statistics are presented in Table 3 for bullet width and cure depth. Those SAM-cure time combinations selected for further investigation are also identified. Representative side profile images for the SAM-cure time combination are shown in Figure 14.

Plots of bullet width vs. curing time and bullet cure depth vs. curing time are presented in Figures 15 and 16. A linear regression analysis of both plots reveals a relatively good fit of the lines for the 0.4 mm SAM (width R^2=0.955 and depth R^2=0.944), but an excellent fit of the lines for the 0.5 mm and 0.25 mm SAMs (width R^2=0.993, depth R^2=0.974 and width R^2=0.982, depth R^2=0.982, respectively).

Theoretical Modeling of the Curing Phenomenon

The semi-major(a) and semi-minor(b) values for all SAM-cure time combinations are presented in Table 4. Substitution into the "y equals" form of the ellipsoid dome equation and consideration of the limiting conditions resulted in x-y scatter plots modeling the 2D curing front profiles. These are presented in Figures 17, 18, and 19. As an example, the curing front of a bullet from a 0.5 mm aperture mask cured for 40 seconds would be modeled by the equation:

$$y = \sqrt{2.139^2 - \frac{2.139^2 x^2}{1.915^2}}$$

and have the limiting conditions of

$$-1.915 \leq x \leq 1.915 \text{ and } 0 \leq y \leq 2.139$$

Scatter plots for the SAM-cure time combinations selected for further investigation are shown in Figure 20.

Plots of bullet width vs. bullet energy (log scale) and bullet cure depth vs. bullet energy (log scale) are presented in Figures 21 and 22. A non-linear regression analysis of both plots reveals an excellent fit of the lines to the logarithmic regression for the 0.5, 0.4, and 0.25 mm SAMs (width R^2=0.98 and depth R^2=0.991, width R^2=0.999 and depth R^2=0.997, and width R^2=0.991 and depth R^2=0.991, respectively).

Representative scatter plot-side profile image overlays for the two models are presented in Figures 23 through 26. Resulting values of D_p, E_c, D_p', and E_c' are listed in Tables 5 and 6. As an example of the predictive model, the curing front profile of a bullet polymerized through a 0.5 mm aperture mask would be described by the equation:

$$y = \sqrt{\left[0.6251 \ln\left(\frac{E}{2.03522}\right)\right]^2 - \frac{\left[0.6251 \ln\left(\frac{E}{2.03522}\right)\right]^2 x^2}{\frac{1}{2}\left[1.1911 \ln\left(\frac{E}{2.59758}\right)\right]^2}}$$

with the limiting conditions of:

$$-\frac{1}{2}\left[1.1911 \ln\left(\frac{E}{2.59758}\right)\right] \leq x \leq \frac{1}{2}\left[1.1911 \ln\left(\frac{E}{2.59758}\right)\right]$$

and

$$0 \leq y \leq 0.6251 \ln\left(\frac{E}{2.03522}\right)$$

where E (the energy applied to the top surface of the specimen) would be dependent upon curing time and the intensity of the light source. A side-by-side comparison and prediction error of the values of *a* and *b* between the measured and predictive models are

listed in Tables 7 and 8. Prediction errors for bullet cure depth ranged from 0.43% (0.5 mm, 20 s) to 3.25% (0.5 mm, 30 s). Prediction errors for bullet radius (½ width) ranged from 0.14% (0.4 mm, 10 s) to 3.78% (0.5 mm, 30 s). The curing nearest the light tip is much wider than the aperture, showing significant side scattering of the light. The curing front profile of the bullet demonstrates the traveling front of the light.

Experimental Groups

Standard and plus mode curing protocols for the SAM-cure time combinations selected for further investigation, as well as the control curing protocol are outlined in Table 9. The energy applied to the top surface for a specimen of a given SAM-cure time combination is also presented for these groups.

Effect on the Degree of Conversion

Summary statistics for top and bottom degree of conversion as well as B/T ratios are presented in Tables 10 through 13, and Figures 27 through 32. Statistical groups are indicated by superscript letters.

For the standard mode of polymerization, the degree of conversion of the top surface of Group G < E and F < B < A, C, and D. The top surface DC of Group C < A. At the bottom surface, the degree of conversion of Groups G and E < F < A, B, C, and D. The bottom surface DC of Groups C and D > B. For the B/T ratio, Group E < B, C, D, F, and G. Group A < B, C, and F, and Group G < C and F.

For the plus mode of polymerization, the degree of conversion of the top surface of Groups A, J, K, L, and M had a significantly higher DC than Groups H and I. At the

bottom surface, Groups J and L had a significantly higher DC than Groups A, H, I, K, and M. The B/T ratio of Groups H, I, J, and L were significantly higher than Groups A and K. There was no significant difference in B/T ratio between Group M and any group.

When comparing a SAM-cure time combination between polymerization modes, the plus mode had a significantly higher top surface DC than the standard mode for combinations of 0.25 mm-20 s (Group E v. K), 0.25 mm-30 s (Group F v. L), and 0.25 mm-40 s (Group G v. M) (Table 11). At the bottom surface, the plus mode also had a significantly higher DC than the 0.25 mm-10 s combination (Group D v. J) (Table 12). The standard and plus modes of polymerization did not have significantly different B/T ratios for any group (Table 13).

Effect on the Knoop Hardness

Summary statistics for top surface Knoop hardness are presented in Tables 14 and 15, and Figures 33 and 34. Statistical groups are indicated by superscript letters.

For the standard mode of polymerization, the top surface KHN of Group G < E and F < B < C and D < A.

For the plus mode of polymerization, Group J had a significantly higher KHN than Groups H, I, and M. Group L had a significantly higher KHN than group H. The KHN of Group A was significantly lower than all groups.

When comparing a SAM-cure time combination between polymerization modes, the plus mode of polymerization had a significantly higher KHN than the standard mode for all groups (Table 15).

Effect on the Polymerization Shrinkage Stress

Summary statistics for the polymerization shrinkage stress are presented in Tables 16 and 17, and Figures 35 and 36. Statistical groups are indicated by superscript letters. As a result of the length of time between testing of the two polymerization modes and the intrinsic sensitivity of the equipment, a second control (A′) for the plus mode was established for purposes of statistical analysis.

For the standard mode of polymerization, the PSS of Group G < F < E < D < B and C < A.

For the plus mode of polymerization, Group M had a significantly lower PSS than Groups H, I, and L. Group J had a significantly lower PSS than Group H, and Group K had a significantly lower PSS than Group L. Group A′ was not significantly different from any of the groups.

The PSS of Group A′ was found to be significantly higher than the PSS of Group A; the control groups were statistically different from each other (Table 17). As a result, comparisons between polymerization modes for a given SAM-cure time combination were not evaluated for PSS.

DISCUSSION AND FUTURE DIRECTIONS

The past work of Chen et al. used a photon migration approach to model energy influx of a dental resin composite [37]. We are the first group to successfully demonstrate and model the curing front profile of a resin composite polymerized by a point light source. The ellipsoid dome model derived from the measured specimens is empirically fit to the curing front profile of the resin bullets. From this model, the Jacobs and Chu et al. models were also fit to the curing front profile to calculate the values of D_p, E_c, D_p', and E_c'. Comparing the results of our study to that of Chen et al., the curvature, or necking, at the base of the bullet is not described by the previous work. This difference is most likely attributed to the presence of the mask in our study and its absence in previous work. The thickness of the mask itself may also have an influence on the scattering effect and traveling front of the light. Variations in aperture size ($ø \leq 0.25$ mm), number and arrangement of apertures, and mask thickness as well as material and their influence on the curing front profile will be key components of future studies. Additional and more detailed approaches to modeling the curing front and the evaluation of these models and those proposed in this study will also be investigated.

Large reductions in degree of conversion (up to 21%) and Knoop hardness (up to 25%) were expected for the standard mode, and observed, due to the lower amount of energy delivered to the surface of the specimens. With regard to the plus mode, a narrow range of conversion (within +/- 3.5%) and Knoop hardness (within +/- 3.5%) were expected, and observed, due to similar energy levels delivered to the surface of the specimens.

One interesting observation is in the specific cases of Groups B, C, H, and I; the B/T degree of conversion ratios were significantly increased as compared to the control. The increase is attributed to a lower top surface degree of conversion while the bottom surface degree of conversion remains similar. This observation indicates that the "pre-cure" area (the base of the bullet) contributes to the lower degree of conversion at the top surface, but not the bottom surface. The lower top surface degree of conversion is interesting especially for Groups H and I which have a full 60 seconds of follow-up polymerization in the plus mode. It is known that not all free radicals generated by the initiation event contribute to polymerization reaction. The efficiency of an initiator is related to the initiating condition and monomer combination. Therefore, there is a corresponding initiator loss in each initiation event. Quite possibly, the pre-curing during bullet formation results in some "waste" of the free radical absorbed by oxygen before the follow-up cure. With two initiating events (initial cure with mask and follow-up without), there would be twice as much waste of the free radical at the surface of the resin composite and therefore result in a lower degree of conversion on the top surface. However, because the light of the first initiating event does not reach the bottom surface of the specimen, it does not result in an initial free radical waste as it does at the top. Only the light energy in the second curing event, which is equivalent to the energy used in the control group, reaches the bottom layer. Therefore a same level of degree of conversion was found at the bottom surface. The implications of this reduced degree of conversion at the top surface with regards to flexural strength, fracture toughness, and polymer structure (ethanol storage test) will be investigated in future studies. Further work exploring the possible "double waste" phenomenon will provide greater insight to

point light source polymerization, but could potentially contribute new insights to our knowledge of the mechanisms leading to the softer top surface commonly documented for soft-start polymerization methods, particularly pulse-delay methods.

The polymerization shrinkage stress experiment was setup to utilize a side curing approach to better mimic the clinical situation. The results, however, were disappointing. Although the PSS for the standard mode significantly decreased as compared to the control, this decrease is more than likely reflective of the accompanying reduced degree of conversions. This is most evident for Groups E, F, and G whose top and bottom surface degree of conversions were significantly less than the other groups. Statistically significant groups were identified for the plus mode of polymerization between the mask-cure time combinations, but with no statistical difference between these groups and the control, conclusions are merely speculative. After calculating the volume ratios of the cured bullet to that of a tensometer specimen, they were found to be in the rage of 0.35% to 3.77%. Such small volume ratios clearly indicate that the amount of cured pre-shrinkage resin composite (the bullet volume) was too low; influence of the bullet on the polymerization shrinkage stress was minimal at best. In future work, the volume ratio could be increased by returning to a bottom-up experimental setup. This switch transforms the measured direction of specimen height from perpendicular to the quartz rods and therefore a fixed height of 6 mm, to parallel with an adjustable specimen height. Reducing the tensometer specimen's height to 3 mm or less would result in volume ratios upwards of 20%. Such an approach will also make it possible to investigate additional SAM-cure time combinations since the limiting factor (bullet width) for the tensometer experiments would increase to 6mm, the diameter of the quartz rods. Investigation of a

wider variety of SAM-cure time combinations will only increase our ability to analyze point light source curing as a potentially novel method of reducing polymerization shrinkage stress of dental resin composites and strengthen proposed conclusions.

As with all early investigations of novel concepts, devices, or materials, this study was exploratory in nature with few, if any published resources available for guidance outside of basic testing methodology. While several conclusions were drawn from the results, the work of this thesis greatly represents an investigation of testing methodology and preliminary stages of optimization in efforts to understand and study the implications of polymerizing dental resin composites with a point light source. Several suggestions for changes and improvements to the experiments have been presented, with many others discussed during the final stages of this project. Implementation of these suggestions and the inclusion of additional experiments are planned for the near future. Despite the disappointing results, through successful demonstration and modeling of the curing phenomenon and observation of subtle changes to Knoop hardness and degree of conversion, we remain confident that point light source polymerization is a novel approach to reducing polymerization shrinkage stress worth continued investigation.

TABLES

Component	Material	WT%	Total Composition
Monomer	Bis-GMA TEGDMA UDMA		30%
Initiator	CQ	0.5	
Co-initiator	DMAEMA	0.25	
Inhibitor	BHT	0.5	
Filler	BBAS		70%

Table 1: Composition of the model resin composite.

Mask	Drill Bit	Aperture ø (mm)	Aperture Area (mm^2)
0.5 mm	#76	0.508	0.196
0.4 mm	#78	0.406	0.126
0.25 mm	#87	0.254	0.049

Table 2: Drill bit and aperture details. Standard drill bits used to create the SAMs and the resulting diameter and area of the apertures.

Mask	Time (s)	Bullet Width (mm)	Bullet Depth (mm)	Test Group
0.5 mm	10	2.119 (0.113)	1.243 (0.080)	☑
	20	2.820 (0.158)	1.673 (0.063)	
	30	3.270 (0.238)	1.873 (0.073)	
	40	3.830 (0.186)	2.139 (0.132)	
0.4 mm	10	1.685 (0.035)	0.940 (0.032)	☑
	20	2.488 (0.060)	1.462 (0.025)	
	30	2.990 (0.059)	1.700 (0.038)	
	40	3.282 (0.087)	1.902 (0.024)	
0.25 mm	10	0.987 (0.048)	0.553 (0.017)	☑
	20	1.474 (0.067)	0.861 (0.057)	☑
	30	1.739 (0.078)	1.027 (0.045)	☑
	40	2.056 (0.072)	1.226 (0.036)	☑

Table 3: Mean(SD) bullet width and depth. Bullet width and depth for all SAM-cure time combinations. Groups selected for further investigation are also indicated.

Mask	Time (s)	Semi-Major (a)	Semi-Minor (b)
0.5 mm	10	1.060	1.243
	20	1.410	1.673
	30	1.635	1.873
	40	1.915	2.139
0.4 mm	10	0.843	0.940
	20	1.244	1.462
	30	1.495	1.700
	40	1.641	1.902
0.25 mm	10	0.494	0.553
	20	0.737	0.861
	30	0.870	1.027
	40	1.028	1.226

Table 4: Semi-major and semi-minor values. Calculated semi-major and semi-minor values for all SAM-cure time combinations.

Mask	D_p	E_c
0.5 mm	0.6251	2.03522
0.4 mm	0.6895	2.35847
0.25 mm	0.4715	1.16202

Table 5: D_p and E_c values. Characteristic penetration depth (D_p) and energy (E_c) values specific to the depth of the cured resin bullet.

Mask	D_p'	E_c'
0.5 mm	1.1911	2.59758
0.4 mm	1.1626	2.20102
0.25 mm	0.7487	1.00643

Table 6: D_p' and E_c' values. Characteristic lateral cure distance (D_p') and energy (E_c') values specific to the width of the cured resin bullet.

Mask	Time	Predicted b	Measured b	Prediction Error (%)
0.5 mm	10	1.235	1.243	0.65
	20	1.680	1.673	0.43
	30	1.934	1.873	3.25
	40	2.114	2.139	1.19
0.4 mm	10	0.953	0.940	1.43
	20	1.455	1.462	0.53
	30	1.734	1.700	1.99
	40	1.933	1.902	1.62
0.25 mm	10	0.542	0.553	1.98
	20	0.869	0.861	0.94
	30	1.060	1.027	3.22
	40	1.196	1.226	2.47

Table 7: Cure depth values (b) derived from mathematical models. Bullet cure depth values derived from both the measured and predicted mathematical models for all SAM-cure time combinations. The prediction error between the two models is also presented.

Mask	Time	Predicted a	Measured a	Prediction Error (%)
0.5 mm	10	1.03172	1.060	2.63
	20	1.45549	1.410	3.23
	30	1.69697	1.635	3.78
	40	1.8683	1.915	2.43
0.4 mm	10	0.8439	0.843	0.14
	20	1.26655	1.244	1.81
	30	1.50225	1.495	0.47
	40	1.66948	1.641	1.73
0.25 mm	10	0.4845	0.494	1.84
	20	0.74398	0.737	0.97
	30	0.89577	0.870	3.02
	40	1.00346	1.028	2.38

Table 8: Bullet radius values (a) derived from mathematical models. Bullet radius values derived from both the measured and predicted mathematical models for all SAM-cure time combinations. The prediction error between the two models is also presented.

Mode	Group	Mask (mm)	Mask Time (s)	No Mask Time (s)	Total Time (s)	Bullet E (mJ)	No Mask E (mJ)	Total Surfac E (mJ)
Control	A	None	0	60	60	0	12689.52	12689.52
Standard	B	0.5	10	50	60	14.69	10574.60	10589.29
	C	0.4	10	50		9.40	10574.60	10584.00
	D	0.25	10	50		3.67	10574.60	10578.27
	E		20	40		7.34	8459.68	8467.02
	F		30	30		11.02	6344.76	6355.78
	G		40	20		14.69	4229.84	4244.53
Plus	H	0.5	10	60	70	14.69	12689.52	12704.21
	I	0.4	10		70	9.40		12698.92
	J	0.25	10		70	3.67		12693.19
	K		20		80	7.34		12696.86
	L		30		90	11.02		12700.54
	M		40		100	14.69		12704.21

Table 9: Curing protocols and top surface energy. Protocols of the control, standard, and plus mode polymerization groups investigated in the study. Energy applied to the top surface is also presented.

Mode	Group	Top DC (%)	Bottom DC (%)	B/T Ratio (%)
Control	A	76.99 (0.98) ^{a,A}	70.15 (2.23) ^{a,b,A}	91.13 (3.13) ^{a,b,A}
Standard	B	70.17 (1.87) ^{b}	68.22 (1.91) ^{a}	97.27 (3.63) ^{c,d}
	C	74.09 (1.38) ^{c}	72.04 (1.65) ^{b}	97.23 (1.58) ^{c}
	D	75.58 (1.86) ^{a,c}	71.37 (1.93) ^{b}	94.51 (4.56) ^{a,c}
	E	66.86 (1.34) ^{d}	59.11 (1.69) ^{c}	88.44 (3.36) ^{b}
	F	64.42 (1.92) ^{d}	63.16 (1.35) ^{d}	98.08 (2.24) ^{c}
	G	60.12 (1.66) ^{e}	57.06 (1.36) ^{c}	94.91 (0.98) ^{a,d}
Plus	H	71.55 (1.90) ^{B}	70.50 (1.97) ^{A}	98.55 (1.77) ^{B}
	I	72.41 (1.36) ^{B}	71.04 (1.74) ^{A}	98.14 (2.68) ^{B}
	J	76.10 (2.21) ^{A}	74.83 (1.14) ^{B}	98.40 (3.54) ^{B}
	K	77.61 (1.82) ^{A}	70.93 (1.69) ^{A}	91.43 (2.60) ^{A}
	L	77.25 (1.95) ^{A}	74.80 (1.97) ^{B}	96.88 (3.72) ^{B}
	M	75.43 (2.31) ^{A}	71.52 (1.87) ^{A}	94.89 (3.96) ^{A,B}

Table 10: Mean(SD) top, bottom, and B/T degree of conversion. Statistical groups are indicated by lowercase (control and standard) or capital (control and plus) superscript letters in each column.

	Group	Standard	Plus
Top DC (%)	0.5 mm-10 s	70.17 (1.87) [a]	71.55 (1.90) [a]
	0.4 mm-10 s	74.09 (1.38) [a]	72.41 (1.36) [a]
	0.25 mm-10 s	75.58 (1.86) [a]	76.10 (2.21) [a]
	0.25 mm-20 s	66.86 (1.34) [a]	77.61 (1.82) [b]
	0.25 mm-30 s	64.42 (1.92) [a]	77.25 (1.95) [b]
	0.25 mm-40 s	60.12 (1.66) [a]	75.43 (2.31) [b]

Table 11: Comparison of top degrees of conversion between modes.

Mean(SD) degrees of conversion on the top surface comparing standard and plus modes. Statistical groups are indicated by lowercase superscript letters in each row.

	Group	Standard	Plus
Bottom DC (%)	0.5 mm-10 s	68.22 (1.91) [a]	70.50 (1.97) [a]
	0.4 mm-10 s	72.04 (1.65) [a]	71.04 (1.74) [a]
	0.25 mm-10 s	71.37 (1.93) [a]	74.83 (1.14) [b]
	0.25 mm-20 s	59.11 (1.69) [a]	70.93 (1.69) [b]
	0.25 mm-30 s	63.16 (1.35) [a]	74.80 (1.97) [b]
	0.25 mm-40 s	57.06 (1.36) [a]	71.52 (1.87) [b]

Table 12: Comparison of bottom degrees of conversion between modes.

Mean(SD) degrees of conversion on the bottom surface comparing standard and plus modes. Statistical groups are indicated by lowercase superscript letters in each row.

	Group	Standard	Plus
B/T Ratio (%)	0.5 mm-10 s	97.27 (3.63) [a]	98.55 (1.77) [a]
	0.4 mm-10 s	97.23 (1.58) [a]	98.14 (2.68) [a]
	0.25 mm-10 s	94.51 (4.56) [a]	98.40 (3.54) [a]
	0.25 mm-20 s	88.44 (3.36) [a]	91.43 (2.60) [a]
	0.25 mm-30 s	98.08 (2.24) [a]	96.88 (3.72) [a]
	0.25 mm-40 s	94.91 (0.98) [a]	94.89 (3.96) [a]

Table 13: Comparison of B/T degree of conversion ratios between modes.

Mean(SD) B/T ratios comparing standard and plus modes. Statistical groups are indicated by lowercase superscript letters in each row.

Mode	Group	KHN (kg/mm^2)
Control	A	52.30 (0.71) ^{a,A}
Standard	B	46.50 (0.53) ^{b}
	C	49.35 (0.76) ^{c}
	D	49.55 (0.84) ^{c}
	E	40.77 (0.84) ^{d}
	F	40.93 (0.51) ^{d}
	G	39.22 (0.47) ^{e}
Plus	H	58.94 (0.52) ^{B}
	I	59.41 (0.57) ^{B,C}
	J	60.78 (0.50) ^{D}
	K	60.12 (0.97) ^{B,C,D}
	L	60.31 (0.88) ^{C,D}
	M	59.61 (0.91) ^{B,C}

Table 14: Mean(SD) top surface Knoop hardness numbers. Statistical groups are indicated by lowercase (control and standard) or capital (control and plus) superscript letters.

	Group	Standard	Plus
KHN (kg/mm^2)	0.5 mm-10 s	46.50 (0.53) [a]	58.94 (0.52) [b]
	0.4 mm-10 s	49.35 (0.76) [a]	59.41 (0.57) [b]
	0.25 mm-10 s	49.55 (0.84) [a]	60.78 (0.50) [b]
	0.25 mm-20 s	40.77 (0.84) [a]	60.12 (0.97) [b]
	0.25 mm-30 s	40.93 (0.51) [a]	60.31 (0.88) [b]
	0.25 mm-40 s	39.22 (0.47) [a]	59.61 (0.91) [b]

Table 15: Comparison of Knoop hardness numbers between modes.

Mean(SD) top surface Knoop hardness numbers comparing standard and plus modes. Statistical groups are indicated by lowercase superscript letters in each row.

Mode	Group	PSS (MPa)
Control	A	2.426 (0.022) [a]
Standard	B	2.226 (0.009) [b]
	C	2.249 (0.026) [b]
	D	2.073 (0.036) [c]
	E	1.690 (0.031) [d]
	F	1.319 (0.010) [e]
	G	0.877 (0.045) [f]
Control′	A′	2.753 (0.139) [A,B,C,D,E]
Plus	H	2.906 (0.169) [A,B]
	I	2.908 (0.212) [A,B,C,D]
	J	2.632 (0.199) [C,D,E]
	K	2.737 (0.049) [A,C,E]
	L	2.811 (0.038) [B,D]
	M	2.588 (0.125) [E]

Table 16: Mean(SD) polymerization shrinkage stress at 30 minutes. Statistical groups are indicated by lowercase (control and standard) or capital (control′ and plus) superscript letters.

	Group	Control (A)	Control′ (A′)
PSS	No Mask	2.426 (0.022) [a]	2.753 (0.139) [b]

Table 17: Comparison of the control group polymerization shrinkage stresses. Mean(SD) polymerization shrinkage stress values for the two controls. Statistical groups are indicated by lowercase superscript letters.

FIGURES

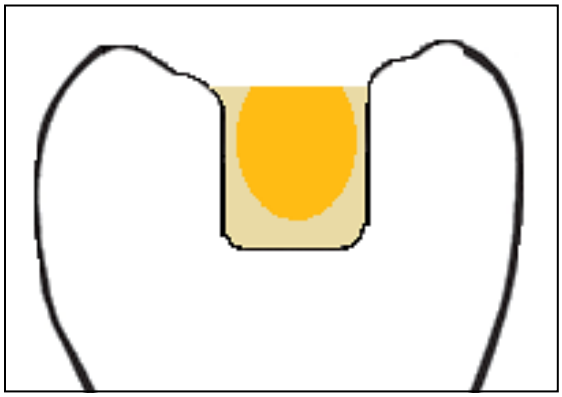

Figure 1: Predicted curing phenomenon beneath a point light source. Side- and top- profiles (left and right, respectively) of the predicted bullet (gold) beneath a point light source, separated from the cavity walls and floor by uncured resin (tan).

Figure 2: Single aperture masks. Left to right, the aperture diameters are 0.5 mm, 0.4 mm, and 0.25 mm respectively.

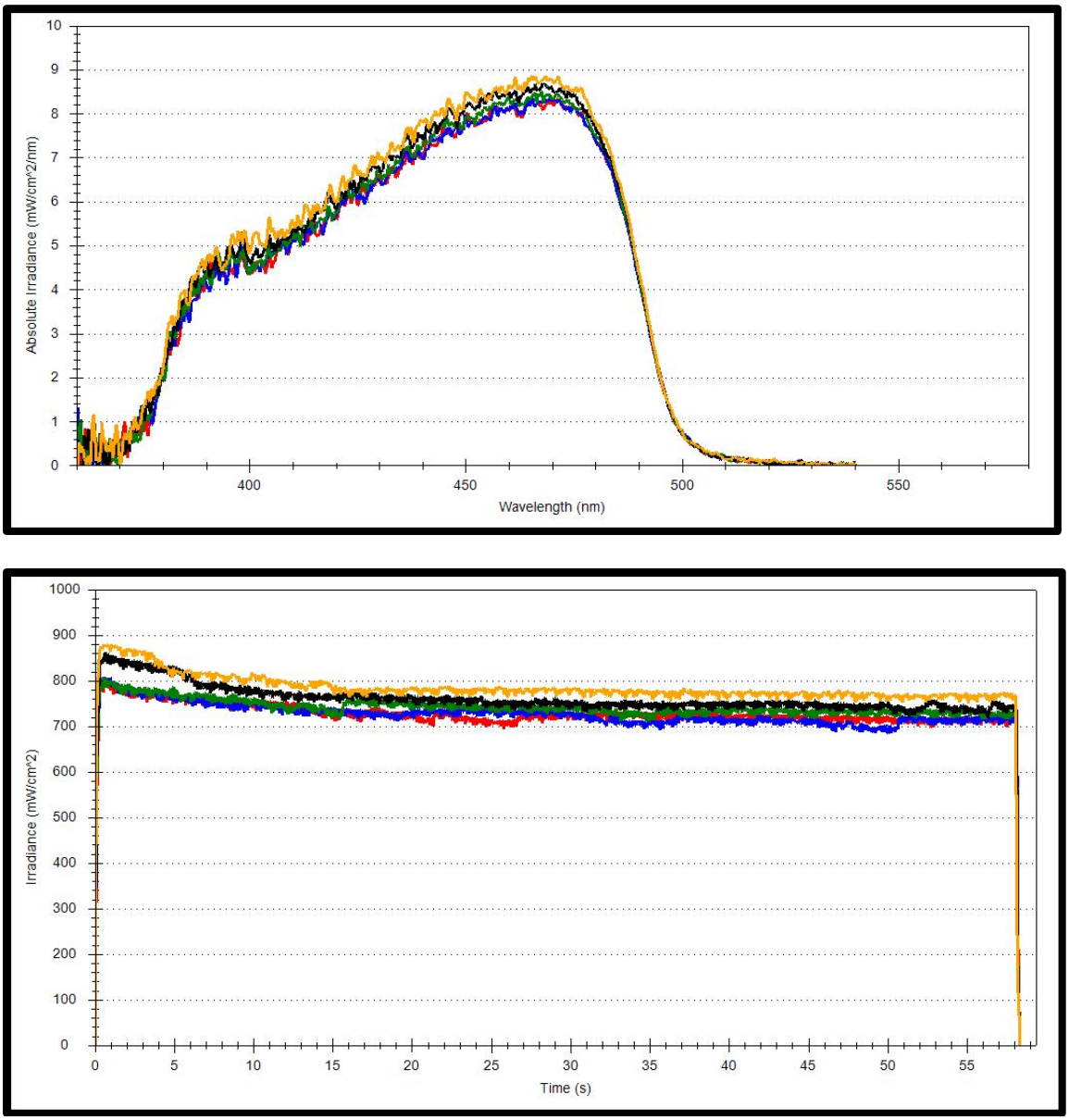

Figure 3: QHL75 spectral range and irradiance. Spectral range (top) and irradiance (bottom) of the QHL75 from the five trial runs.

Figure 4: Experimental setup to investigate point light source curing.

Arrangement of the glass slides, resin filled mold, and single aperture mask.

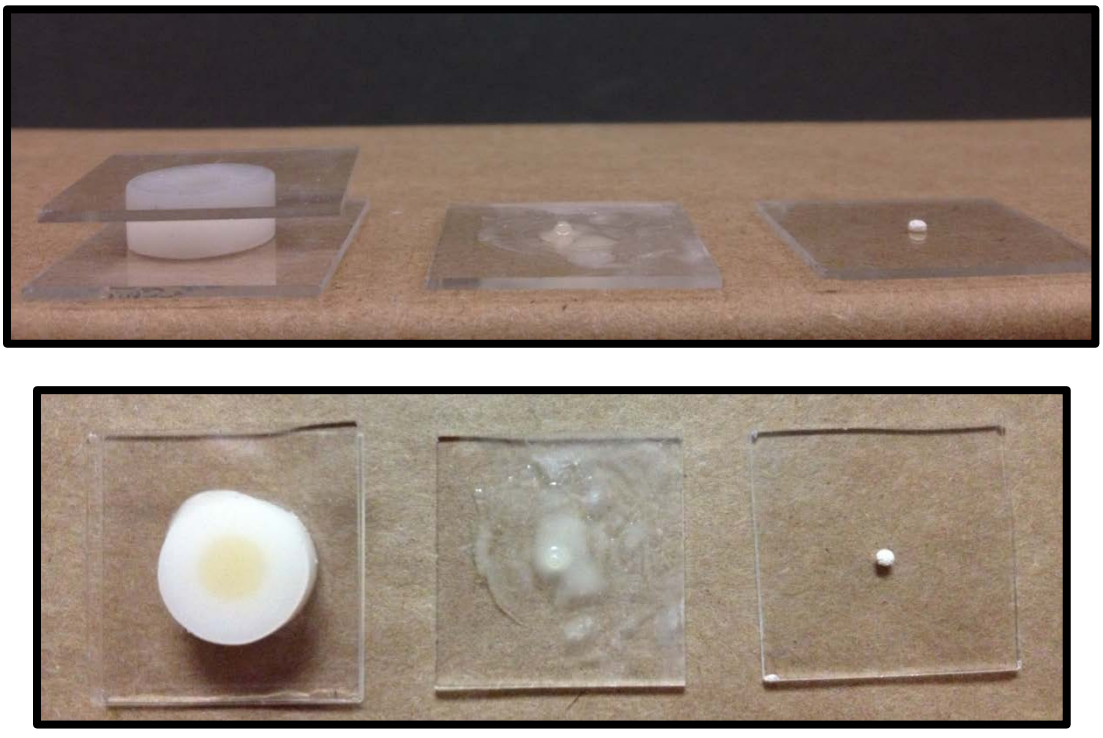

Figure 5: Stages of exposing the cured resin bullet. Side (top) and overhead (bottom) views of the stages of exposing the cured resin bullet.

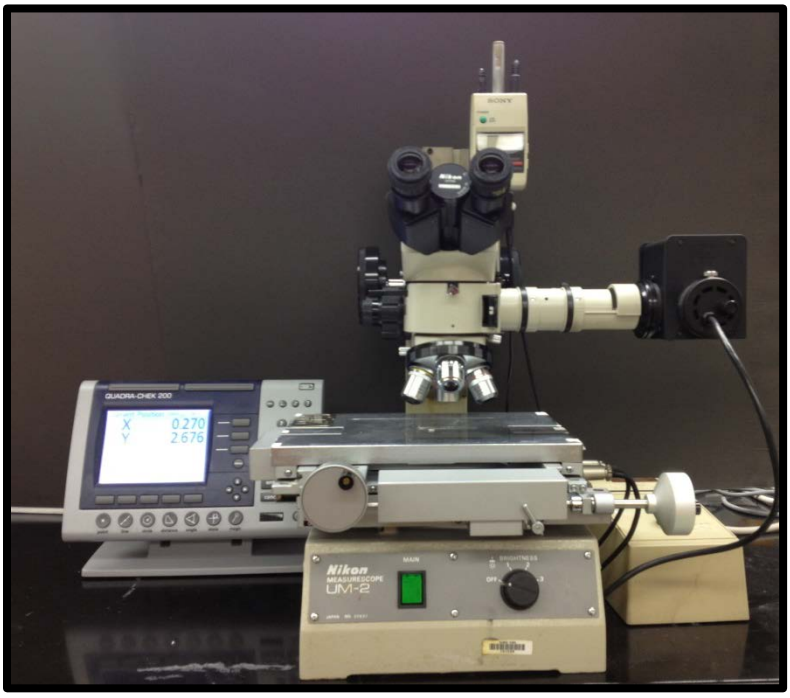

Figure 6: Measurescope and digital readout system. Instrument used to measure the cured resin bullet dimensions.

Figure 7: PocketGoniometer. Instrument used to image the side profiles of the cured resin bullets.

Figure 8: FTIR. Instrument (top) used to measure the degree of conversion. The ZnSe crystal and mounting assembly for such measurements (bottom).

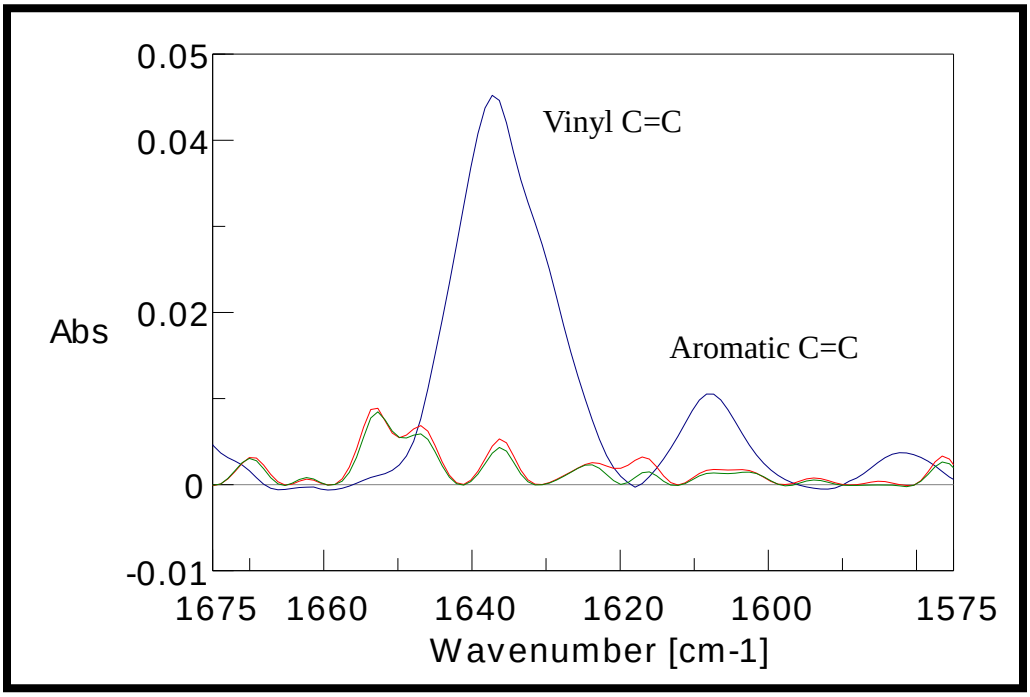

Figure 9: Representative degree of conversion curves. Overlay of representative curves from an uncured (blue), top surface (red), and bottom surface (green) of a specimen from the control group. The vinyl C=C (1638 cm^{-1}) and aromatic C=C (1608 cm^{-1}) are also identified.

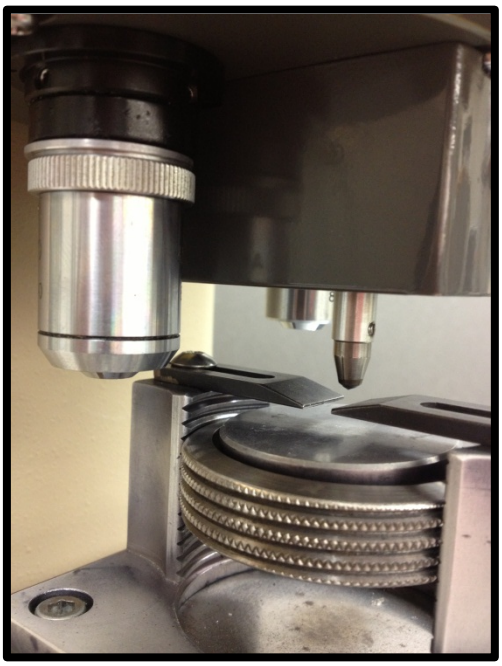

Figure 10: Knoop hardness tester. The hardness tester (top) and its loading platform (bottom) with the 20x eyepiece and Knoop indenter for determining the hardness numbers of a specimen.

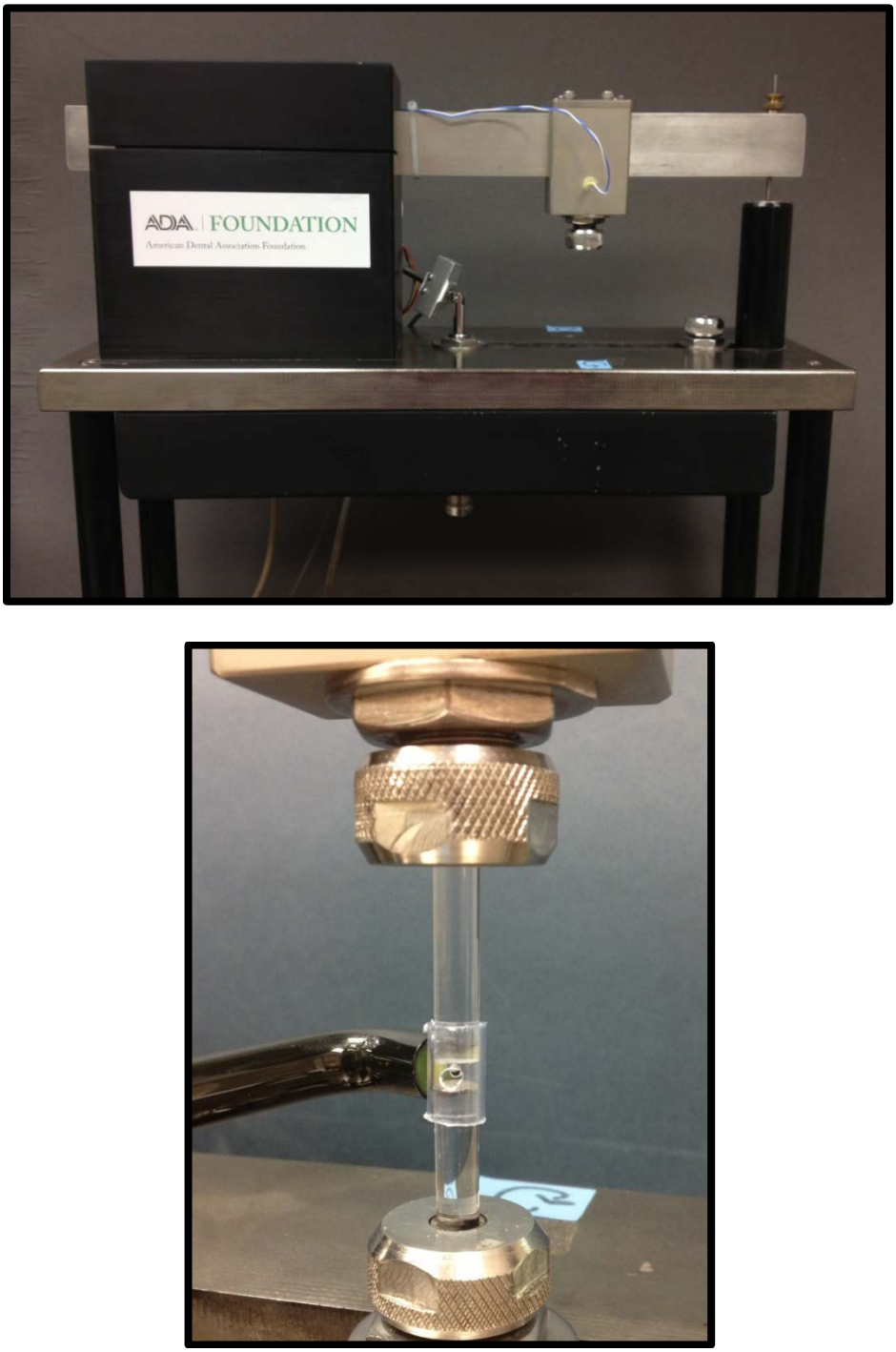

Figure 11: ADA tensometer. Instrument (top) for the measurement of polymerization shrinkage stress. The side curing approach testing setup for this study (bottom) with quartz rods, plastic tube, and curing light in position.

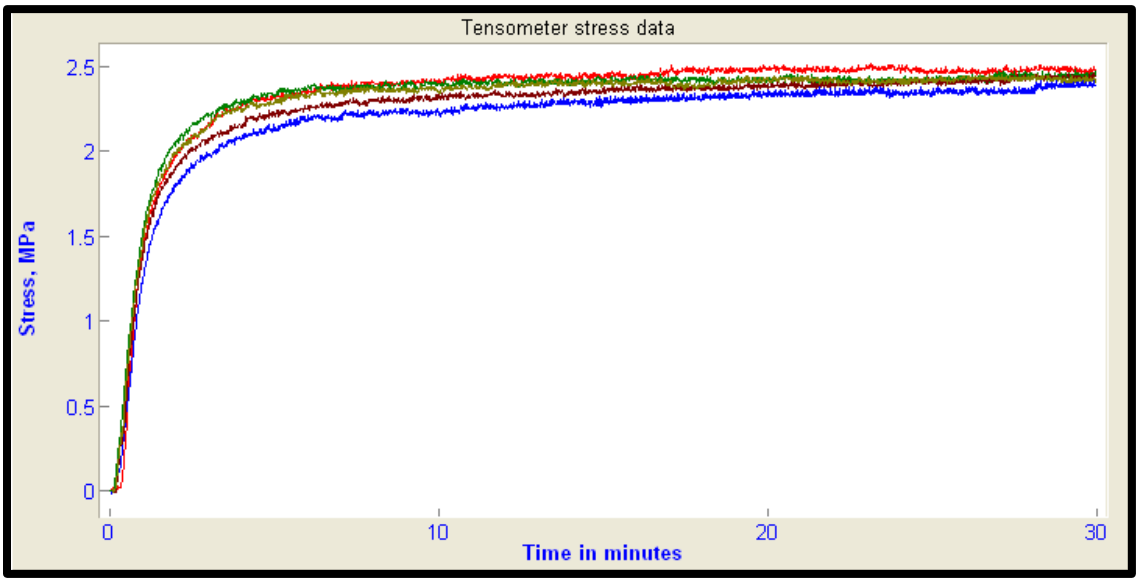

Figure 12: Representative shrinkage stress vs. time curves. Representative curves for the model resin composite.

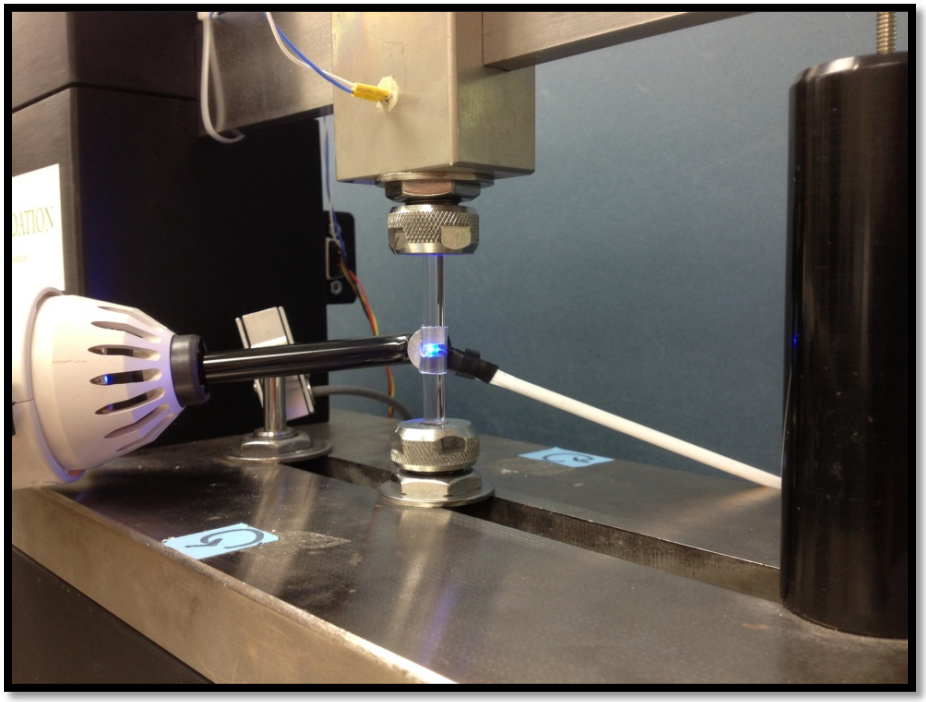

Figure 13: Experimental setup for side curing. Setup for polymerization with a single aperture mask in position before filling the space between the two quartz rods with the model resin composite.

Figure 14: Representative side profile images of cured resin bullets.

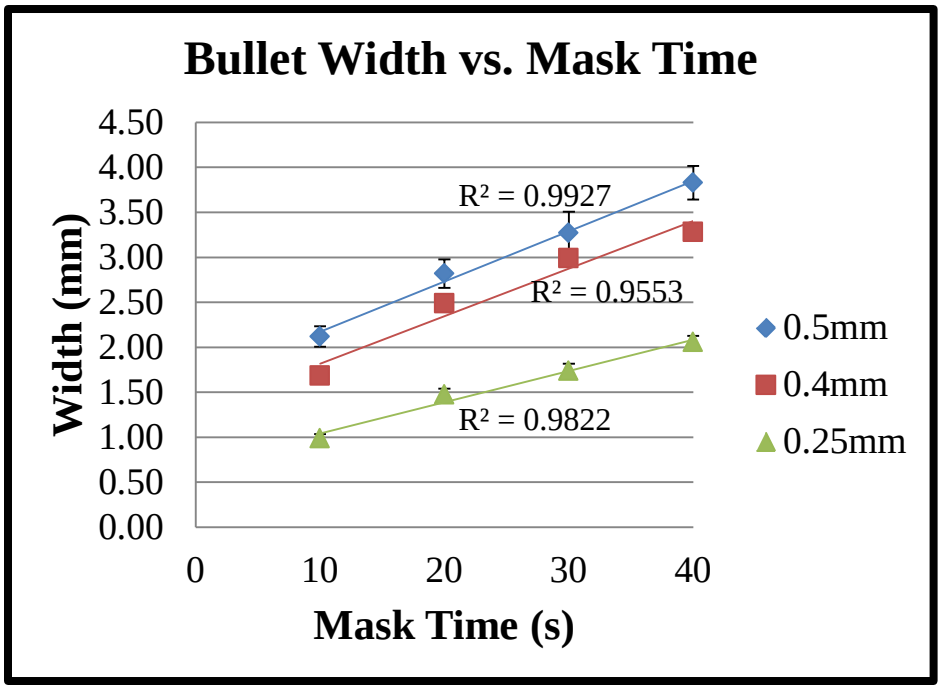

Figure 15: Linear regression analysis of width vs. time.

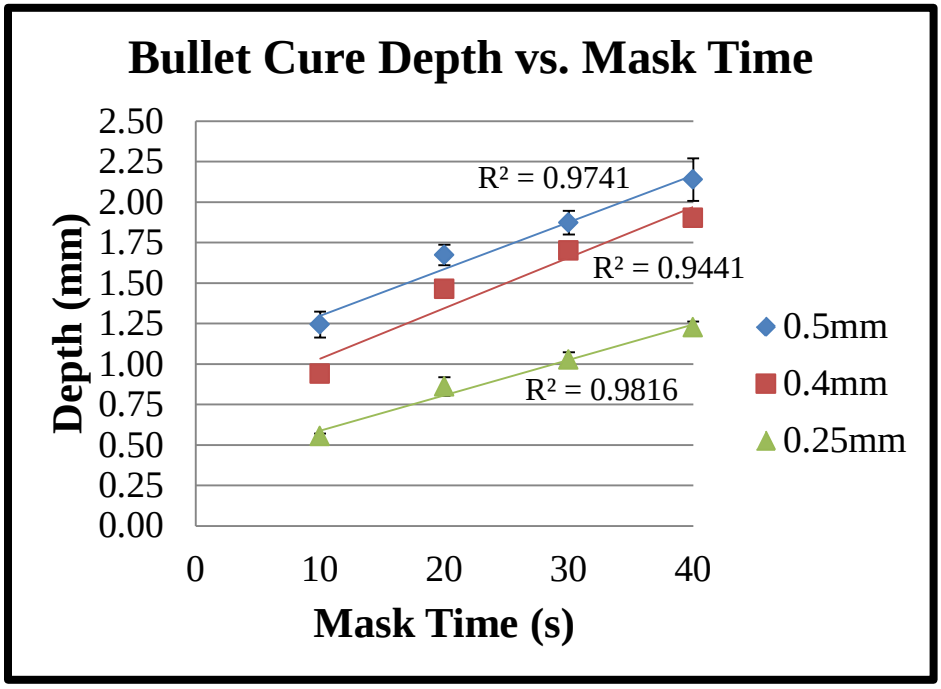

Figure 16: Linear regression analysis of cure depth vs. time.

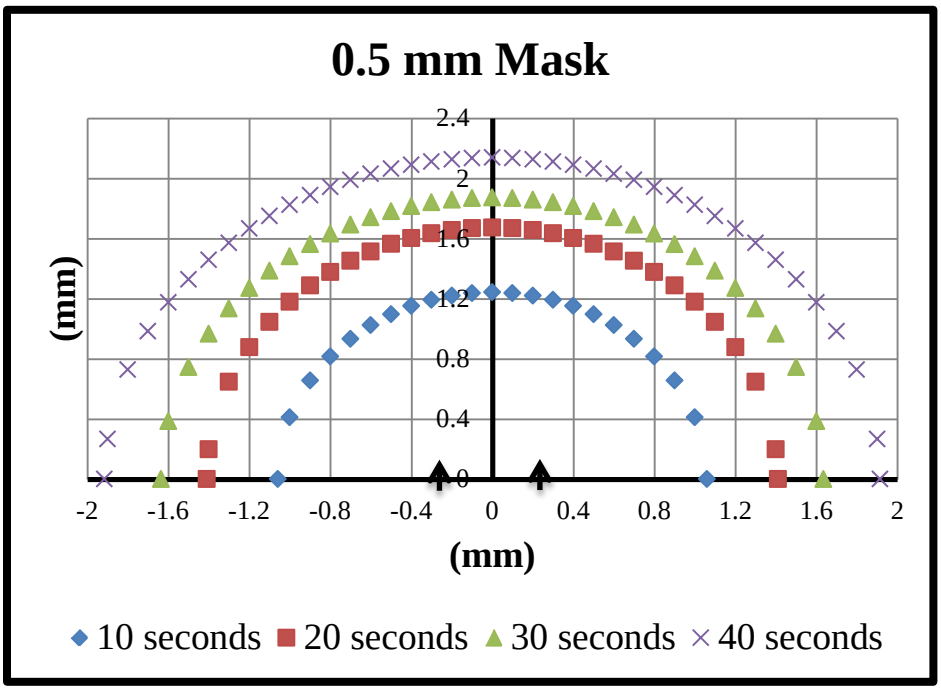

Figure 17: 0.5 mm mask x-y scatter plots. Scatter plots modeling the curing front of a resin bullet. The boundaries of the aperture are represented by black arrows along the x-axis.

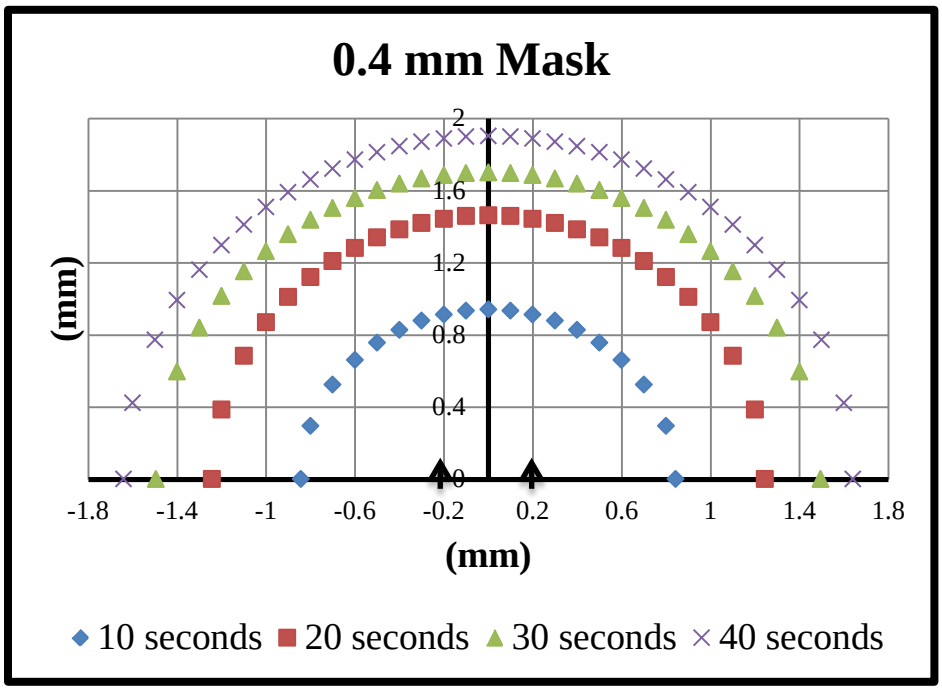

Figure 18: 0.4 mm mask x-y scatter plots. Scatter plots modeling the curing front of a resin bullet. The boundaries of the aperture are represented by black arrows along the x-axis.

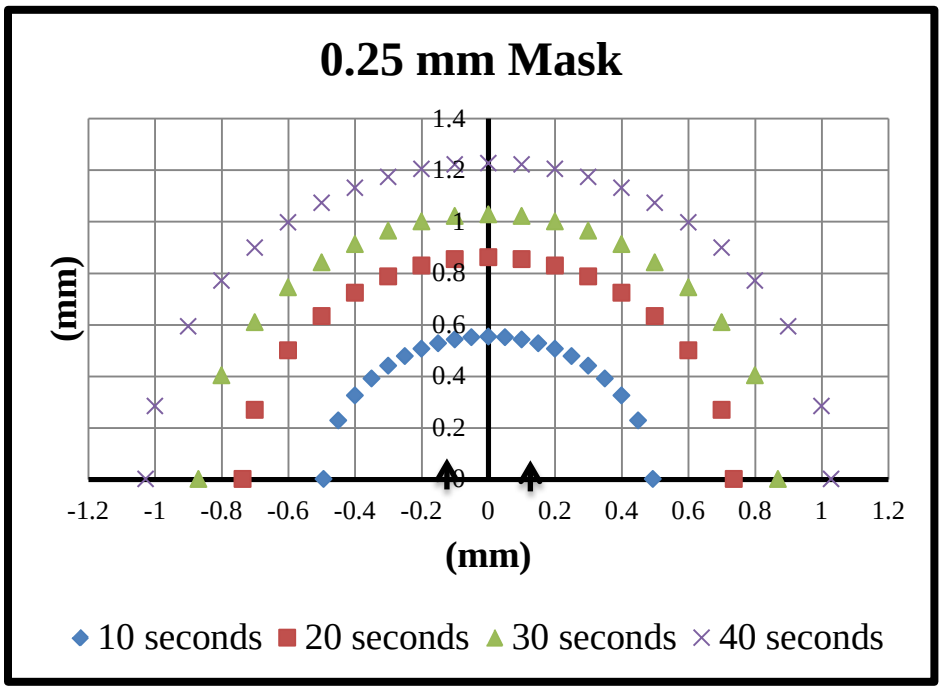

Figure 19: 0.25 mm mask x-y scatter plots. Scatter plots modeling the curing front of a resin bullet. The boundaries of the aperture are represented by black arrows along the x-axis.

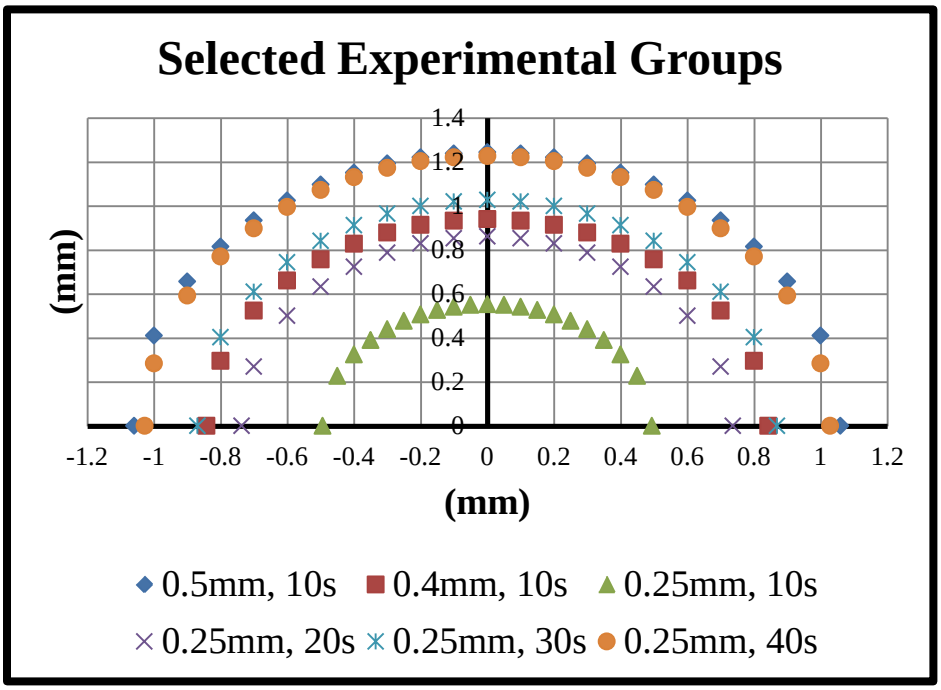

Figure 20: Scatter plots of investigated SAM-cure time combinations.

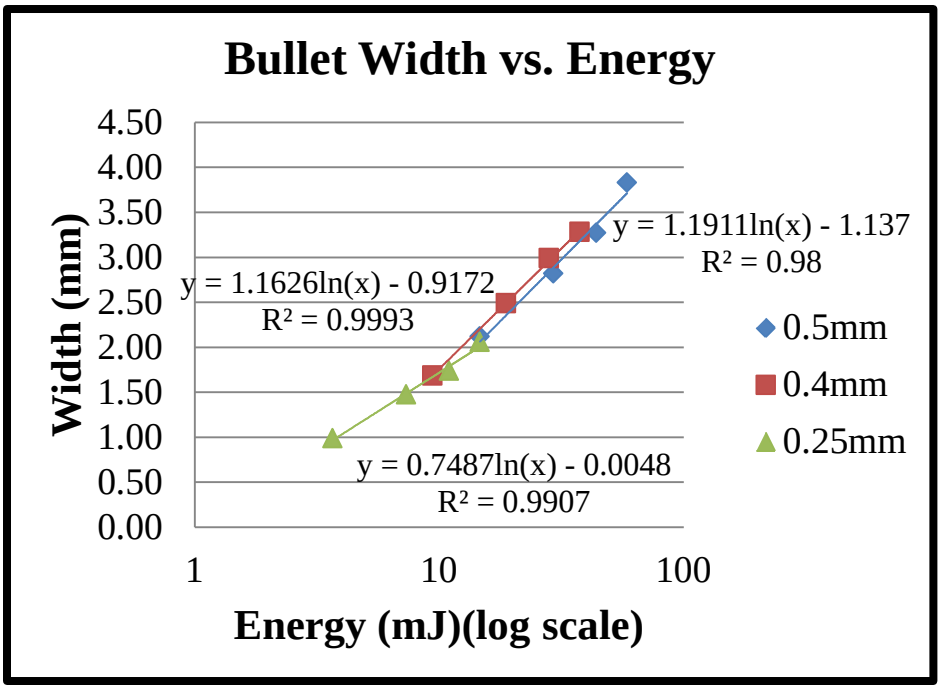

Figure 21: Non-linear regression analysis of bullet width vs. energy.

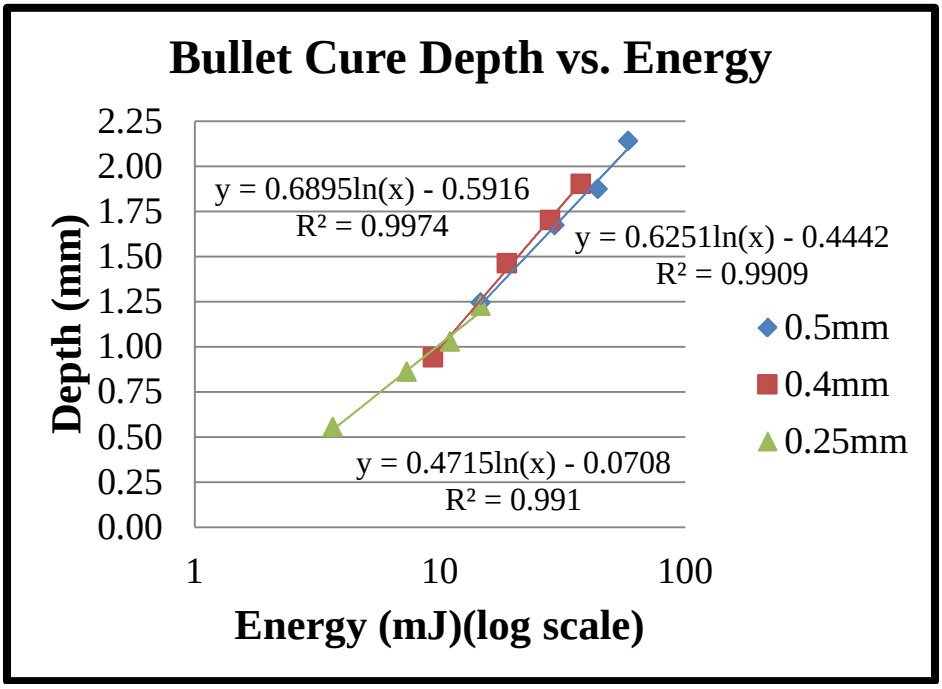

Figure 22: Non-linear regression analysis of bullet cure depth vs. energy.

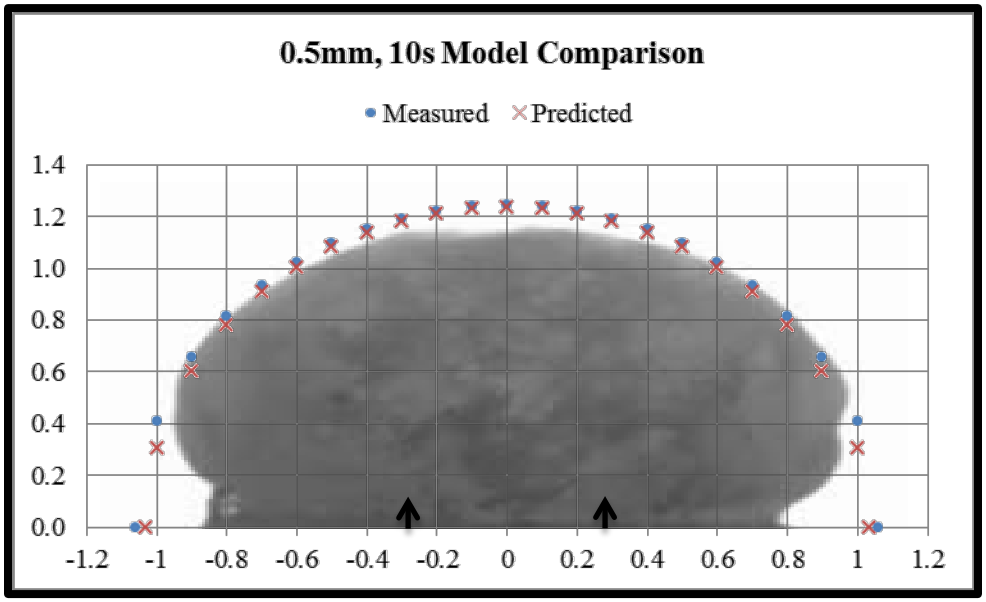

Figure 23: 0.5 mm, 10 second model scatter plot-side profile overlay. Scatter plot-side profile overlay of the mathematical models for a 0.5 mm mask and curing time of 10 seconds. Boundaries of the aperture are represented by black arrows along the x-axis.

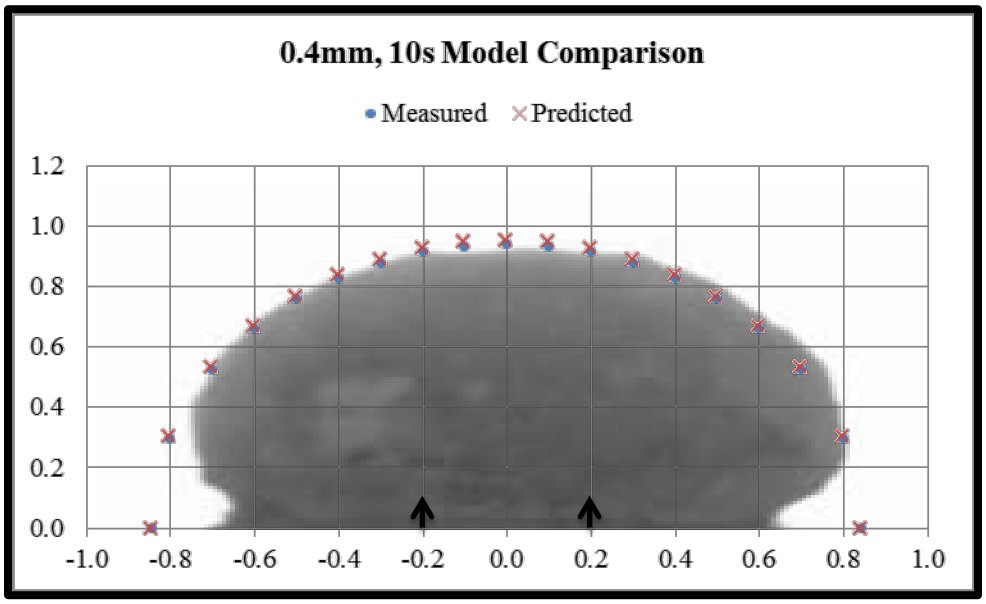

Figure 24: 0.4 mm, 10 second model scatter plot-side profile overlay. Scatter plot-side profile overlay of the mathematical models for a 0.4 mm mask and curing time of 10 seconds. Boundaries of the aperture are represented by black arrows along the x-axis.

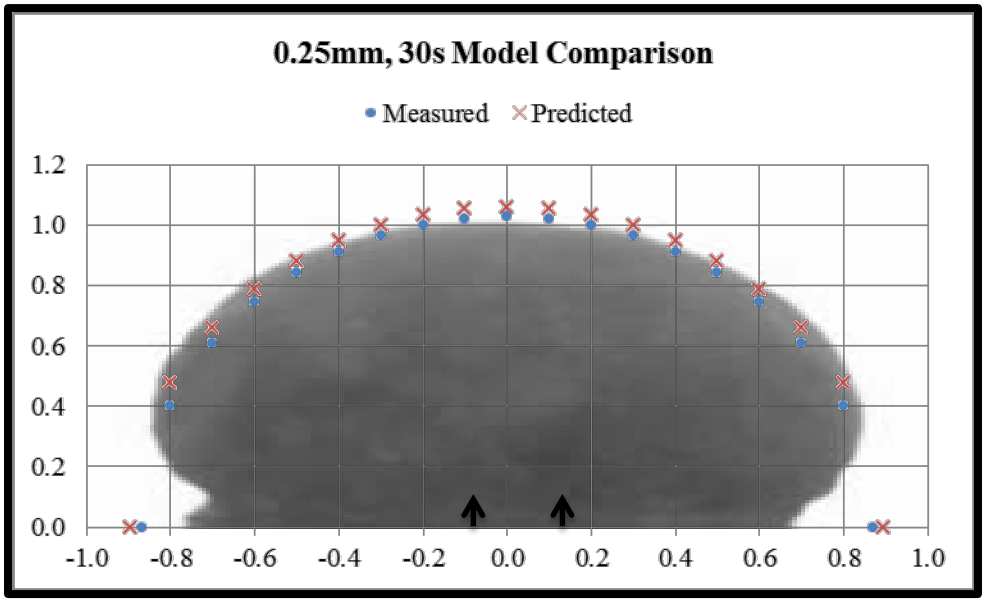

Figure 25: 0.25 mm, 30 second model scatter plot-side profile overlay.

Scatter plot-side profile overlay of the mathematical models for a 0.25 mm mask and curing time of 30 seconds. Boundaries of the aperture are represented by black arrows along the x-axis.

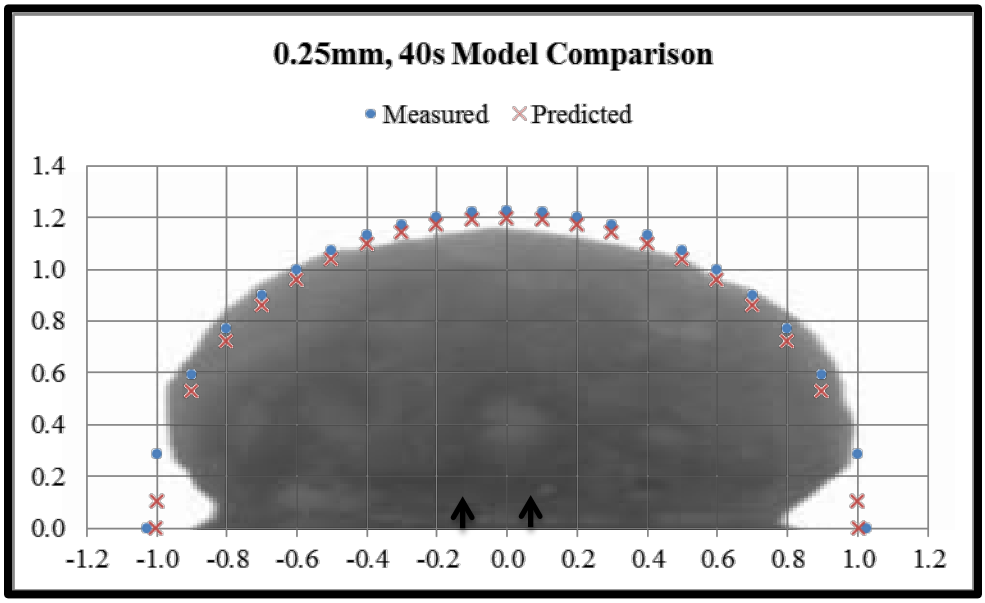

Figure 26: 0.25 mm, 40 second model scatter plot-side profile overlay.

Scatter plot-side profile overlay of the mathematical models for a 0.25 mm mask and curing time of 40 seconds. Boundaries of the aperture are represented by black arrows along the x-axis.

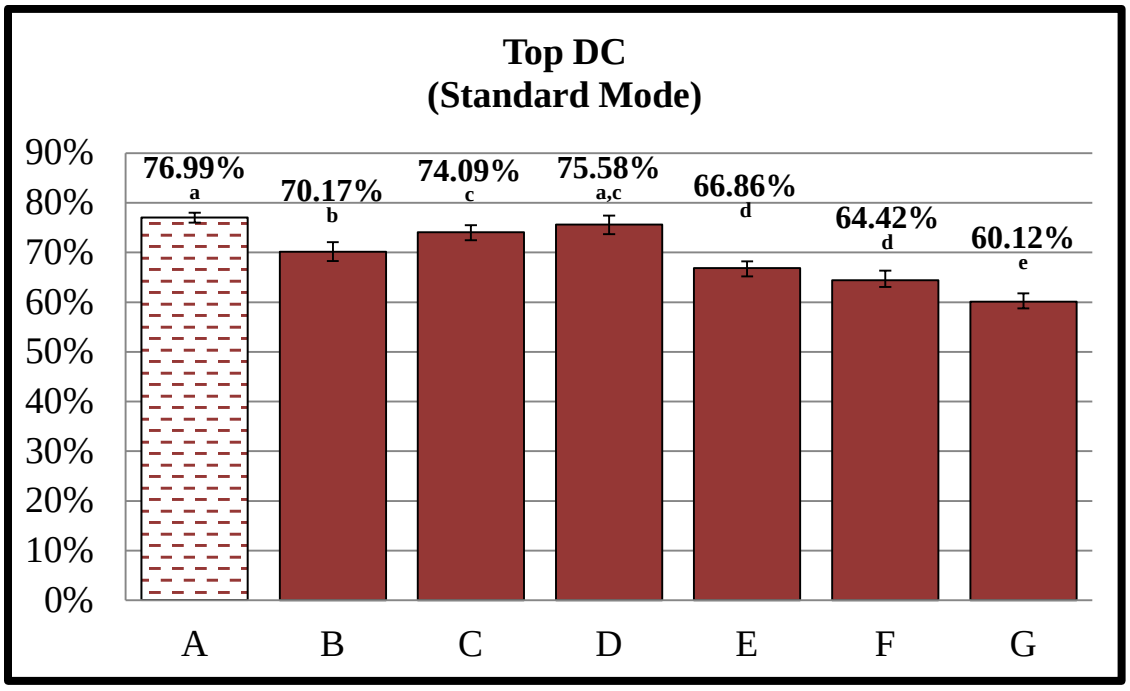

Figure 27: Standard mode mean top degree of conversions. Degree of conversion at the top surface of specimens cured using the standard mode or with no mask (control). Statistical groups are indicated by lowercase letters.

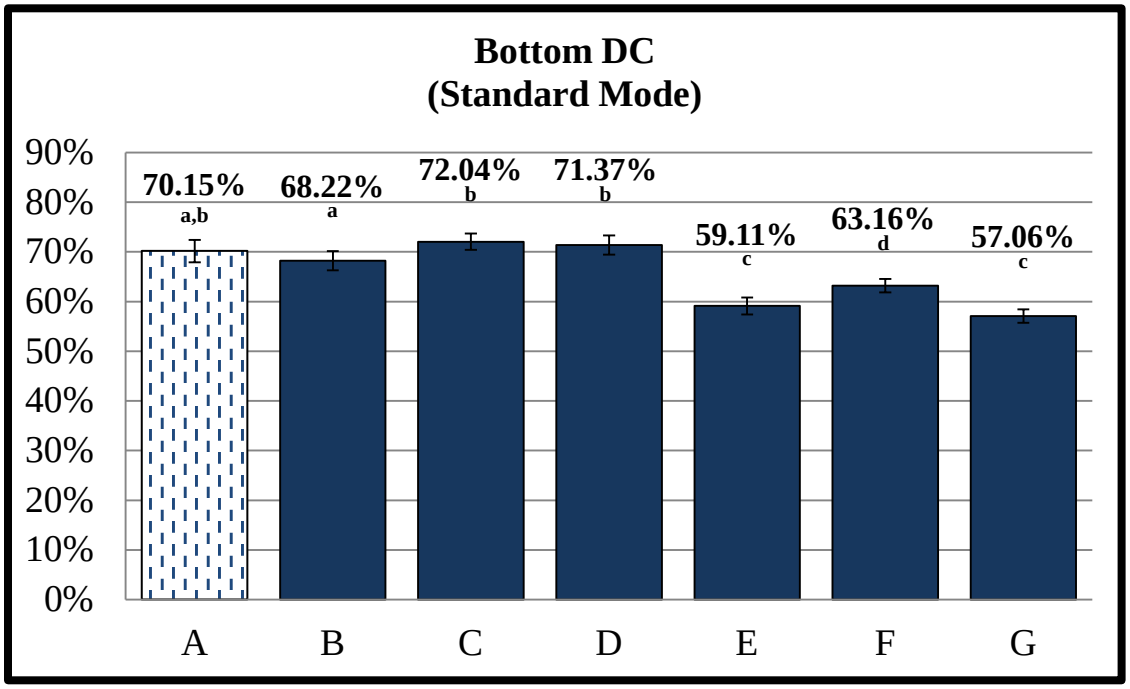

Figure 28: Standard mode mean bottom degree of conversions. Degree of conversion at the bottom surface of specimens cured using the standard mode or with no mask (control). Statistical groups are indicated by lowercase letters.

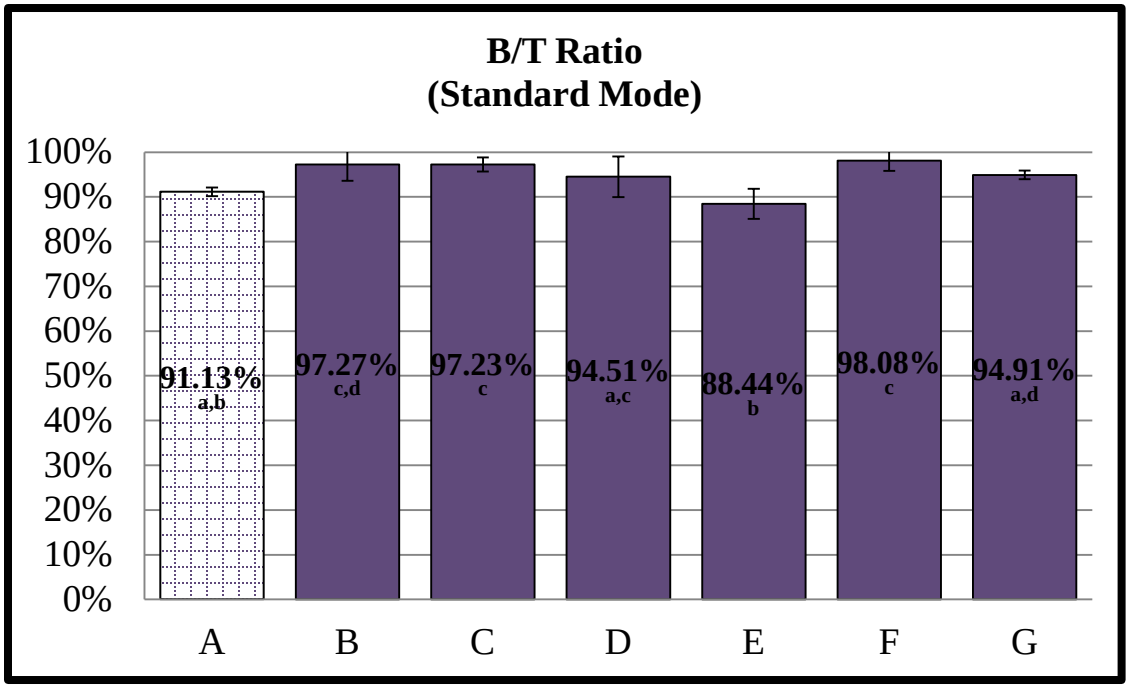

Figure 29: Standard mode mean bottom/top degree of conversion ratios. Bottom/top degree of conversion ratios of specimens cured using the standard mode or with no mask (control). Statistical groups are indicated by lowercase letters.

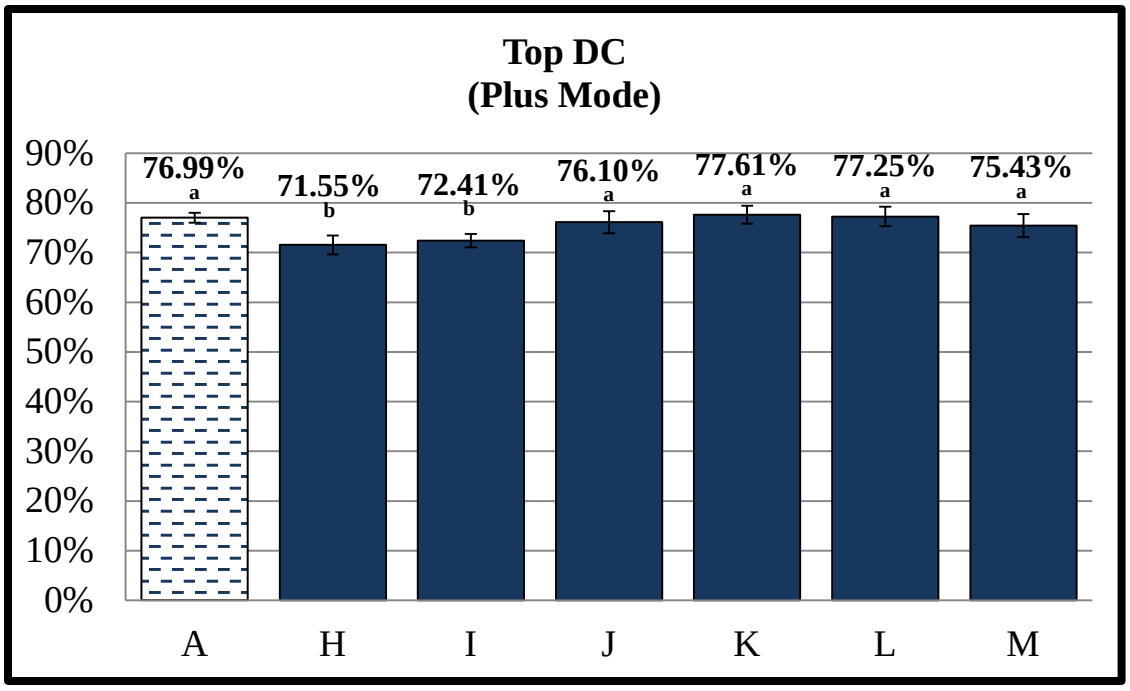

Figure 30: Plus mode mean top degree of conversions. Degree of conversion at the top surface of specimens cured using the plus mode or with no mask (control). Statistical groups are indicated by lowercase letters.

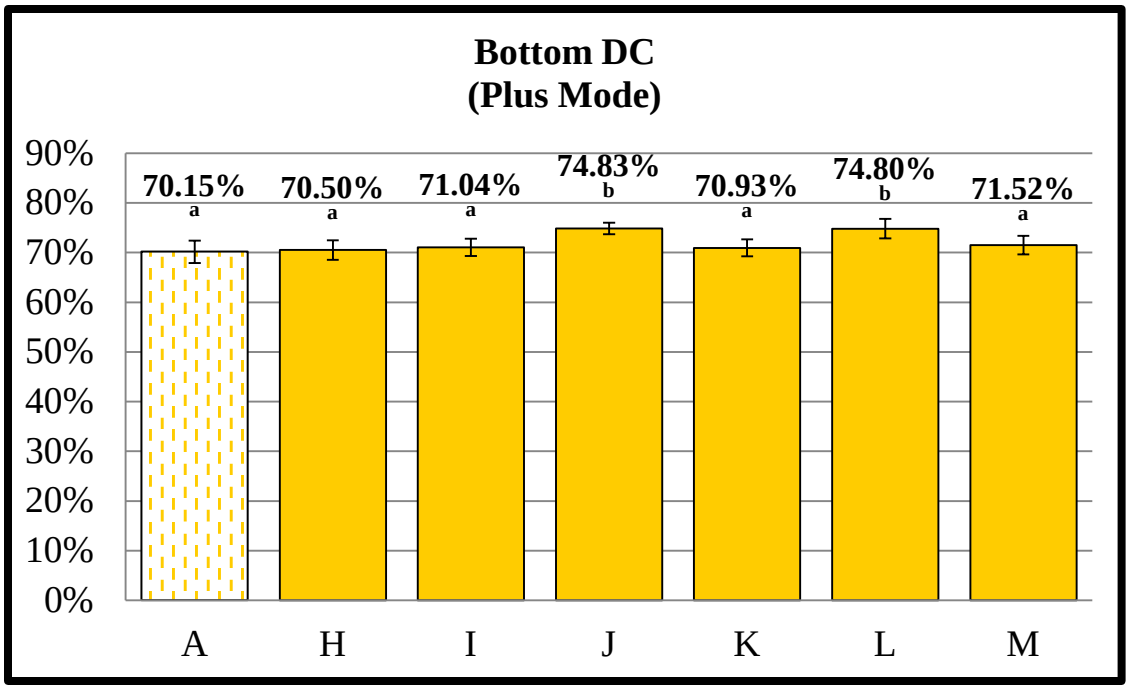

Figure 31: Plus mode mean bottom degree of conversions. Degree of conversion at the bottom surface of specimens cured using the plus mode or with no mask (control). Statistical groups are indicated by lowercase letters.

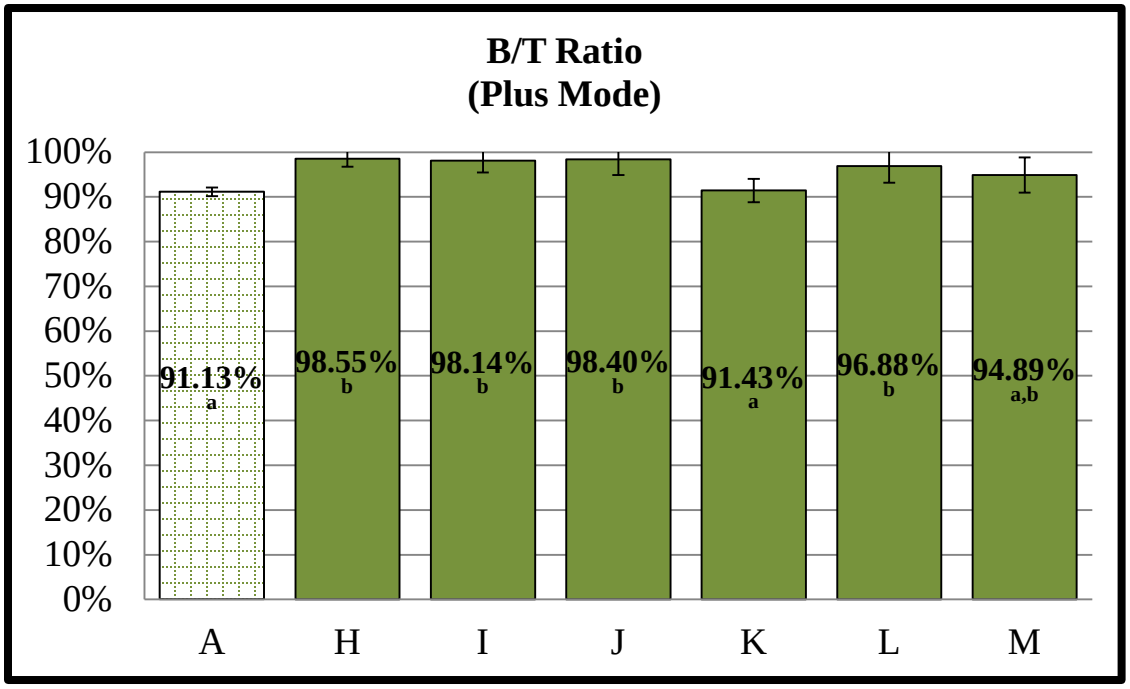

Figure 32: Plus mode mean bottom/top degree of conversion ratios.

Bottom/top degree of conversion ratios of specimens cured using the plus mode or with no mask (control). Statistical groups are indicated by lowercase letters.

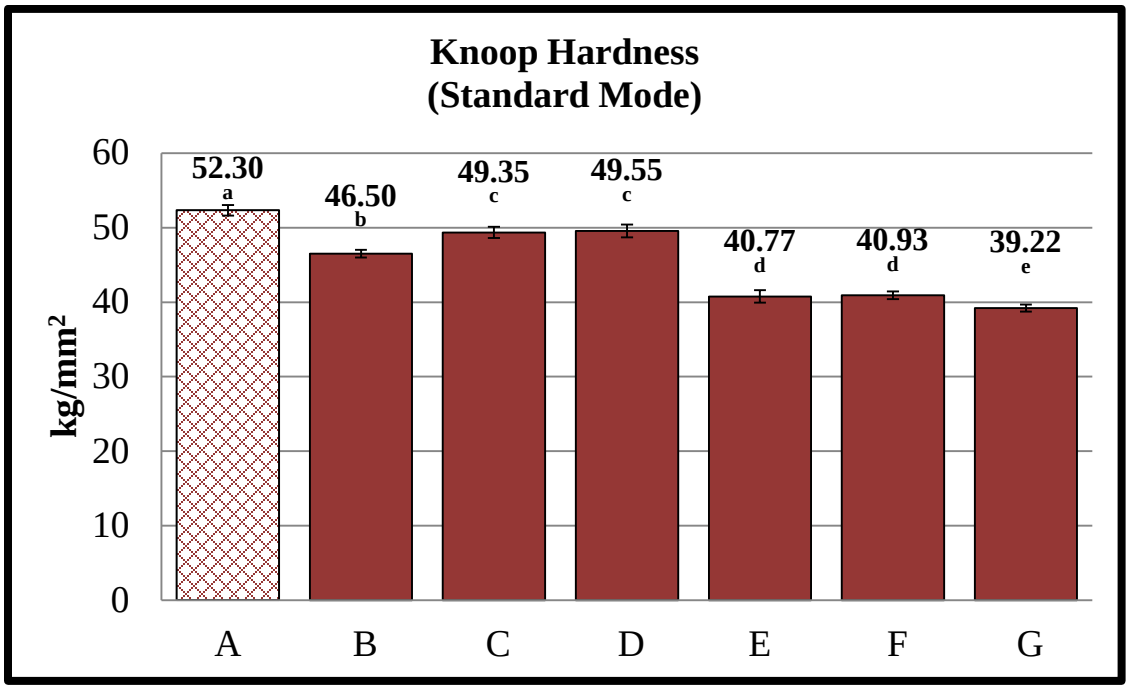

Figure 33: Standard mode mean Knoop hardness numbers. Knoop hardness numbers at the top surface of specimens cured using the standard mode or with no mask (control). Statistical groups are indicated by lowercase letters.

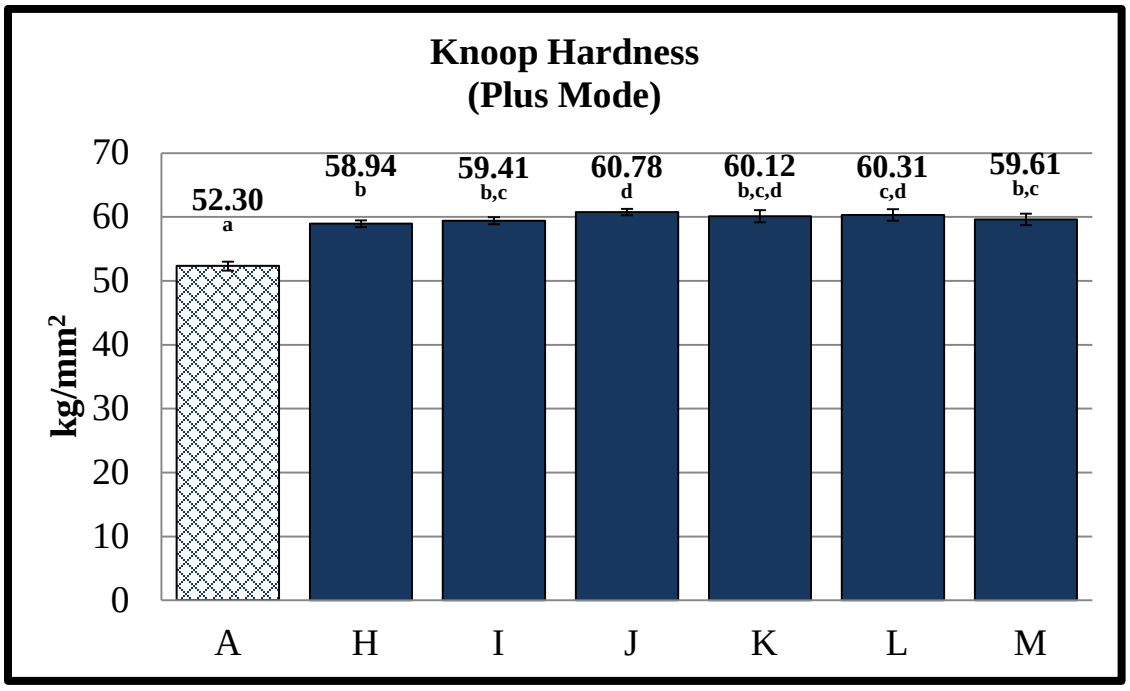

Figure 34: Plus mode mean Knoop hardness numbers. Knoop hardness numbers at the top surface of specimens cured using the plus mode or with no mask (control). Statistical groups are indicated by lowercase letters.

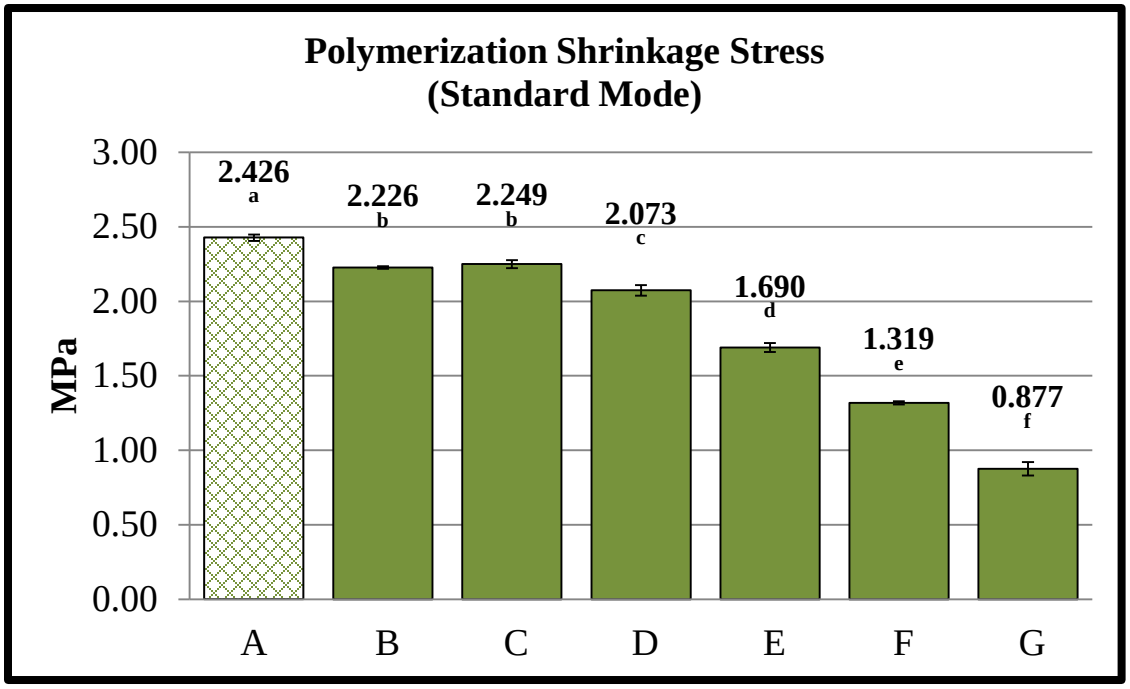

Figure 35: Standard mode mean shrinkage stresses at 30 minutes.

Polymerization shrinkage stresses for specimens cured using the standard mode or with no mask (control). Statistical groups are indicated by lowercase letters.

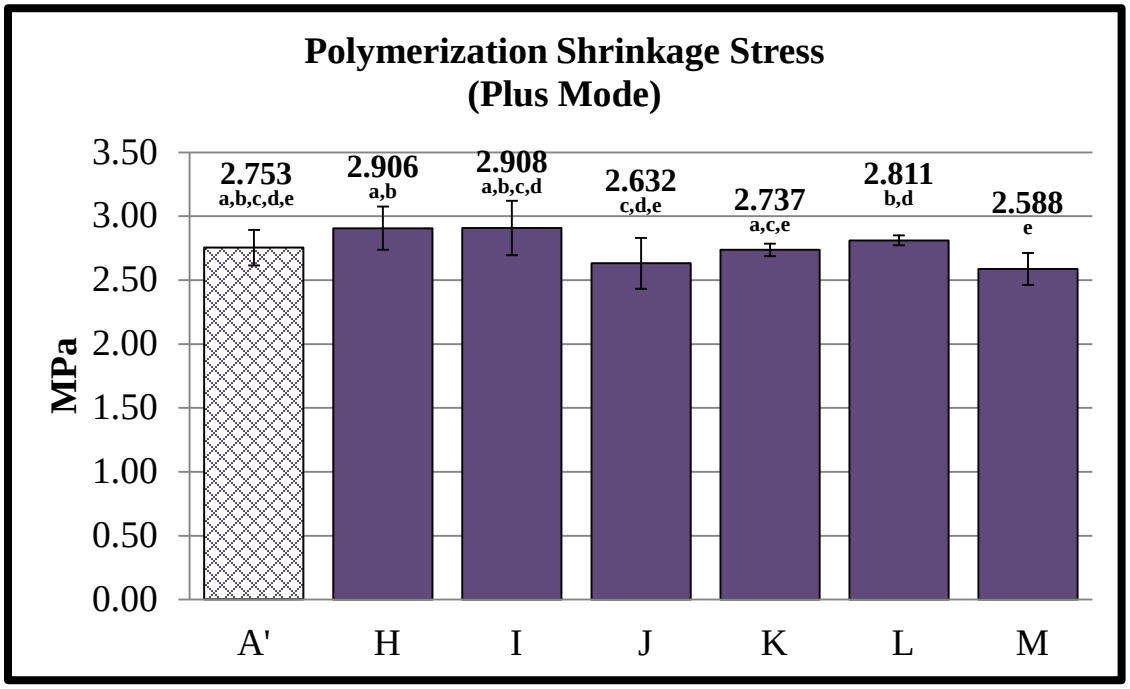

Figure 36: Plus mode mean shrinkage stresses at 30 minutes. Polymerization shrinkage stresses for specimens cured using the plus mode or with no mask (alternate control). Statistical groups are indicated by lowercase letters.

REFERENCES

1. Bowen RL. Adhesive bonding of various materials to hard tooth tissues. VI. Forces developing in direct filling materials during hardening. JADA. 1967;74(3):439-445.

2. Bowen RL, Rapson JE, Dickson G. Hardening shrinkage and hygroscopic expansion of composite resins. J Dent Res. 1982;61(5):654-658.

3. Bowen RL, Nemoto K, Rapson JE. Adhesive bonding of various materials to hard tooth tissues: forces developing in composite materials during hardening. JADA. 1983;106(4):475-477.

4. Davidson CL, DeGee AJ. Relaxation of polymerization contraction stresses by flow in dental composites. J Dent Res. 1984;63(2):146-148.

5. Davidson CL, DeGee AJ, Feilzer AJ. Competition between the composite-dentin bond strength and the polymerization contraction stress. J Dent Res. 1984;63(12):1396-1399.

6. Davidson CL, Feilzer AJ. Polymerization shrinkage and polymerization shrinkage stress in polymer-based restoratives. J Dent. 1997;25(6):435-440.

7. Schneider LFJ, Cavalcante LM, Silikas N. Shrinkage stresses generated during resin-composite applications: a review. J Dent Biomech. 2010.

8. Ferracane JL. Developing a more complete understanding of stresses produced in dental composites during polymerization. Dent Mater J. 2005;21(1):36-42.

9. Visvanathan A, Ilie N, Hickel R, Kunzelmann KH. The influence of curing times and light curing methods on the polymerization shrinkage stress of a shrinkage-optimized composite with hybrid-type prepolymer fillers. Dent Mater J. 2007;23(7):777-784.

10. Pires-de-souza F, Drubi Filho B, Casemiro LA, Garcia LFR, Consani S. Polymerization shrinkage stress of composites photoactivated by different light sources. Braz Dent J. 2009;20(4):319-324.

11. Charton C, Colon P, Pla F. Shrinkage stress in light-cured composite resins: influence of material and photoactivation mode. Dent Mater J. 2007;23(8):911-920.

12. Braga RR, Ferracane JL. Contraction stress related to degree of conversion and reaction kinetics. J Dent Res. 2002;81(2):114-118.

13. Lim BS, Ferracane JL, Sakaguchi RL, Condon JR. Reduction of polymerization contraction stress for dental composites by two-step light activation. Dent Mater J. 2002;18(6):436-444.

14. Braga RR, Ballester RY, Ferracane JL. Factors involved in the development of polymerization shrinkage stress in resin-composites: a systematic review. Dent Mater J. 2005;21(10):962-970.

15. Lu H, Stansbury JW, Bowman CN. Impact of curing protocol on conversion and shrinkage stress. J Dent Res. 2005;84(9):822-826.

16. Stansbury JW, Trujillo-Lemon M, Lu H, Ding X, Lin Y, Ge J. Conversion-dependent shrinkage stress and strain in dental resins and composites. Dent Mater J. 2005;21(1):56-67.

17. Cunha LG, Alonso RCB, Neves ACC, de Goes MF, Ferracane JL, Sinhoreti MAC. Degree of conversion and contraction stress development of a resin composite irradiated using halogen and LED at two C-factor levels. Oper Dent. 2009;34(1):24-31.

18. Braga RR, Ferracane JL. Alternatives in polymerization contraction stress management. CROBM. 2004;15:176-184.

19. Lu H, Stansbury JW, Bowman CN. Towards the elucidation of shrinkage stress development and relaxation in dental composites. Dent Mater J. 204;20(10):979-986.

20. Versluis A, Tantbirojn D. Theoretical considerations of contraction stress. Compend Contin Educ Dent Suppl. 1999;25:S24-32.

21. Karthick K, Sivakumar K, Geetha Priya PR, Shankar S. Polymerization shrinkage composites- a review. JIADS. 2011;2(2):32-36.

22. Ilie N, Jelen E, Hickel R. Is the soft-start polymerization concept still relevant for modern curing units? Clin Oral Invest. 2011;15:21-29.

23. Pfeifer CSC, Braga RR, Ferracane JL. Pulse-delay curing: influence of initial irradiance and delay time on shrinkage stress and microhardness of restorative composites. Oper Dent. 2006;31(5):610-615.

24. Cunha LG, Alonso RCB, de Souza-Junior EJC, Neves ACEC, Correr-Sobrinho L, Sinhoreti MAC. Influence of the curing method on the post-polymerization shrinkage stress of a composite resin. J Appl Oral Sci. 2008;16(4):266-270.

25. Asmussen E, Peutzfeldt A. Influence of pulse-delay curing on softening of polymer structures. J Dent Res. 2001;80(6):1570-1573.

26. Feng L, Suh BI. A mechanism on why slower polymerization of a dental composite produces lower contraction stress. J. Biomed. Mater. Res., Part B. 2006;78(1):63-69.

27. Ilie N, Felten K, Trixner K, Hickel R, Kunzelmann KH. Shrinkage behavior of a resin-based composite irradiated with modern curing units. Dent Mater J. 2005;21(5):483-489.

28. Pfeifer CS, Ferracane JL, Sakaguchi RL, Braga RR. Factors affecting photopolymerization stress in dental composites. J Dent Res. 2008;87(11):1043-1047.

29. Calheiros FC, Daronch M, Rueggeberg FA, Braga RR. Influence of irradiant energy on degree of conversion, polymerization rate and shrinkage stress in an experimental resin composite system. Dent Mater J. 2008;24(9):1164-1168.

30. Young RJ, Lovell PA. 1991. Introduction to polymers. [Internet]. Second Edition. New York(NY):Chapman & Hall.

31. Musanje L, Darvell BW. Curing-light attenuation in filled-resin restorative materials. Dent Mater J. 2006;22(9):804-817.

32. Aravamudhan K, Rakowski D, Fan PL. Variation of depth of cure and intensity with distance using LED curing lights. Dent Mater J. 2006;22(11):988-994.

33. Aravamudhan K, Floyd CJE, Rakowski D, Flaim G, Dickens S, Eichmiller FC, Fan PL. Light-emitting diode curing light irradiance and polymerization of resin-based composite. JADA. 2006;137(2):213-223.

34. Rueggeberg FA, Caughman WF, Curtis JW, Davis HC. A predictive model for the polymerization of photo-activated resin composites. Int J Prosthodont. 1994;7(2):159-166.

35. Cohen ME, Leonad DL, Charlton DG, Roberts HW, Ragain JC. Statistical estimation of resin composite polymerization sufficiency using microhardness. Dent Mater J. 2004;20(2):158-166.

36. Emami N, Sjödahl M, Söderholm KJM. How filler properties, filler fraction, sample thickness and light source affect light attenuation in particulate filled resin composites. Dent Mater J. 2005;21(8):721-730.

37. Chen YC, Ferracane JL, Prahl SA. A pilot study of a simple photon migration model for predicting depth of cure in dental composite. Dent Mater J. 2005;21(11):1075-1086.

38. Cook WD. Factors affecting the depth of cure of UV-polymerizied composites. J Dent Res. 1980;59(5):800-808.

39. Kawaguchi M, Fukushima T, Miyazaki K. The relationship between cure depth and transmission coefficient of visible-light-activated resin composites. J Dent Res. 1994;73(2):516-521.

40. Racz LM, Li L, Abedian B. Cure kinetics of light-activated polymers. J Polym Sci B: Polym Phys. 1998;36(16):2887-2894.

41. Jacobs PF. 1992. Rapid prototyping & manufacturing: fundamentals of stereolithography. Dearborn(MI):Society of Manufacturing Engineers.

42. Chu TM, Halloran JW, Wagner W. Ultraviolet curing of highly loaded hydroxyapatite suspension. In: Rusin RP, Fischman GS. Bioceramics: materials and applications II. Ceramic Transactions Vol. 63. Westerville (OH): The American Ceramic Society;1995. p.57-66.

CURRICULUM VITAE

Meoghan Elizabeth MacPherson

EDUCATION

Master of Science, Dental Materials — June 2013
Thesis Mentor: Tien-Min Gabriel Chu, D.D.S, Ph.D.
Indiana University
Indiana University-Purdue University Indianapolis, Indianapolis, IN

Bachelor of Science in Engineering, Bioengineering — May 2005
University of Pennsylvania, Philadelphia, PA

PROFESSIONAL EXPERIENCE

Laboratory Manager and Research Analyst — Nov. 2011 – July 2013
Acting Laboratory Manager — July 2008 – Nov. 2011
Laboratory Technician/Research Assistant — Sep. 2007 – July 2008
Dental Biomaterials Lab
Indiana University School of Dentistry

Research Technician — Mar. 2007 – Sep. 2007
Oral Health Research Institute
Indiana University School of Dentistry

Research Assistant — Nov. 2006 – Jan. 2007
Department of Nephrology
Indiana University School of Medicine

Patent Examiner — July 2005 – Aug. 2006
Dental Art Unit
United States Patent & Trademark Office

PUBLICATIONS

JA Platt, PE Reifeis, **ME MacPherson**, LH Willis, ML Kirkup, B Rhodes, and DT Brown. The Battle of the Bonds. *Journal of the Indiana Dental Association*, 2012 Summer; 91(2): 20-22.

AC Mackey, RL Karlinsey, TG Chu, **ME MacPherson**, DL Alge. Development of Niobium Oxide Coatings on Sand-Blasted Titanium Alloy Dental Implants. *Materials Sciences and Applications*, 2012; 3: 301-305.

CONFERENCE POSTERS

M.E. MacPherson, J.A. Platt, and T.G. Chu. Polymerization Through Single Apertures: Curing-Front Profiles and Degree of Conversion. Submitted to the 2013 General Session & Exhibition of the International Association for Dental Research. March 20-23, Seattle, WA.

G. Gomez, R. Huang, **M.E. MacPherson**, A. Ferreira Zandona, R.L. Gregory. Photo Inactivation of Early *Streptococcus mutans* Biofilm by Blue Light. Submitted to the 2013 General Session & Exhibition of the International Association for Dental Research. March 20-23, Seattle, WA.

A.C.O. Souza, D. Souza, **M.E. MacPherson**, S.M. Rode, J. Platt, and A.L.S. Borges. Shrinkage and Hygroscopic Expansion of Composite-Resins: Analysis Video-Imaging Technique. Submitted to the 2013 General Session & Exhibition of the International Association for Dental Research. March 20-23, Seattle, WA.

W.D. Browning, **M.E. MacPherson**, and J.A. Platt. Tear Strength of Five Hydrophilic PVS Impression Materials. Submitted to the 2013 General Session & Exhibition of the International Association for Dental Research. March 20-23, Seattle, WA.

J.A. Platt, **M. MacPherson**, and B. Rhodes. Polish Retention of a Nanohybrid Flowable Composite. 2011 General Session & Exhibition of the International Association for Dental Research. March 16-19, San Diego, CA.

J. Platt, **M. MacPherson**, and B. Rhodes. Polymerization Shrinkage and Contraction Stress of an Experimental Composite. 2010 Annual Meeting & Exhibition of the American Association for Dental Research. March 3-6, Washington, DC.

PROFESSIONAL SOCIETY MEMBERSHIPS

Academy of Dental Materials (ADM)
American Association for Dental Research (AADR)
Association for Women in Science (AWIS)
International Association for Dental Research (IADR)